ELSEVIER

Comput. Methods Appl. Mech. Engrg. 173 (1999) 71–98

Computer methods in applied mechanics and engineering

Elastoplastic materials with martensitic phase transition and twinning at finite strains: numerical solution with the finite element method

Alexander V. Idesman, Valery I. Levitas, Erwin Stein*

Institute of Structural and Computational Mechanics, University of Hannover, Appelstrasse 9A, D-30167 Hannover, Germany

Received 16 April 1999

Dedicated to Professor Peter Haupt on the occasion of his 60th birthday.

Abstract

A new quasistatic problem formulation and finite element (FE) algorithm for martensitic phase transition (PT) and twinning in elastoplastic materials at large strains, based on a recently proposed thermomechanical approach [1,2] are presented. The instantaneous occurrence of PT in some region based on thermodynamics, without introduction of volume fraction and prescribing the kinetic equations for it, is considered. Stress history dependence during the transformation process is a characteristic feature of the PT criterion. The deformation model is based on the multiplicative decomposition of the total deformation gradient into elastic, transformation and plastic parts and the generalization of Prandtl–Reuss equations to the case of large strains and PT. The case of small elastic, but large plastic and transformation strains is assumed. For numerical simulation of PT the 'inverse' problem is considered, i.e. the position and size of the PT region (nucleus) are prescribed in advance, and then the condition for PT is defined from the PT criterion. Such an approach includes a finite element solution of the elastoplastic problem with the prescribed transformation deformation gradient and the changing elastoplastic properties in the transforming region during PT. The usage of the current configuration and the true Cauchy stresses along with assumptions of small elastic strains and zero modified plastic spin allows us to use—with small modifications—the radial return algorithm and the consistent elastoplastic moduli for the case of small strains. Some modifications of the iterative algorithm related to the numerical integration of constitutive equations along with the radial return algorithm are suggested in order to improve the accuracy of solutions for large increments of external load (such modifications can be used for any elastoplastic problem without phase transition as well). The model problems of nucleation at shear–band intersection and appearance of a single martensitic plate and a single twin are solved and analyzed.

1. Introduction

Many modern technologies include PT in elastoplastic materials. Thermomechanical treatment of materials involves consecutively or simultaneously occurring PT and plastic straining, which result in the required microstructure and the physical–mechanical properties. Strain induced PT and transformation induced plasticity (TRIP) are other important examples.

Martensitic PT in elastoplastic materials is a complex thermomechanical process accompanied by the change of mechanical properties, transformation strain and a complicated distribution of local stresses and strains. The difficulties of a thermomechanical description of PT are related to definition of the PT condition, the formulation of boundary–value problems and their numerical solution. We consider the instantaneous occurrence of PT in some region based on thermodynamics, without introducing volume fraction and prescribing the kinetic equations for it. This allows us to study fundamental problems of martensite and twin nucleation and its

*Corresponding author. E-mail: stein@leibniz.ibnm.uni-hannover.de

0045-7825/99/$ – see front matter
PII: S0045-7825(98)00258-8

subsequent growth in a grain as well as microstructure formation. There are only a few known numerical approaches for such type of PT in elastoplastic materials for small strains (see [3–7]).

Usually, transformation and plastic strains are finite and a corresponding general theory for PT and twinning (as a particular case of PT) was developed by Levitas [1,2]. The condition of nucleation includes—in contrast to known approaches—the history of local stress variation in nucleus during the transformation process. Therefore, knowledge of stresses and strains before and after PT does not give sufficient information for calculating the PT condition. For determination of some unknown parameters during PT, the corresponding extremum principle for PT is used.

The aim of the paper is to present algorithmic and computational aspects of implementation of a simple isotropic deformation model for description of PT and twinning in elastoplastic materials at finite strains. The model is based on the multiplicative decomposition of the total deformation gradient into elastic, transformation and plastic parts and the generalization of Prandtl–Reuss equations to the case of large strains and PT. The modified plastic deformation rate considered is conjugate to the Cauchy stress. The structure of constitutive equations is similar for the cases of small and large strains. It is necessary to say that the generalization of Prandtl–Reuss equations to the case of large strains even without PT is not unique. It depends on the choice of a measure for the plastic deformation rate and some assumptions with respect to the calculation of the plastic spin. For example, the approaches presented in [8,9] and [10,11] give different generalizations for the case of finite strains. As the available experimental data for large elastoplastic strains are confined, a possible reason for choosing one or other approach can be the simplicity of its numerical treatment. So, in this paper we have modified the measure of plastic deformation rate (Eq. (17)) in comparison with our first papers on PT simulations at finite strains [12,13] from computational point of view. We should note that an alternative possibility for description of PT in elastoplastic materials is to use single crystal plasticity. But we do not consider it here because such an approach would be far more complicated for numerical implementation.

For numerical solution of PT we consider the 'inverse' problem, i.e. the position and size of the PT region (nucleus) are prescribed in advance, and then the condition for PT is defined from the PT criterion. Such an approach includes the solution of elastoplastic problems with the prescribed transformation deformation gradient and the changing elastoplastic properties in transforming region during PT. Formally it is similar to solution of thermoelastoplastic problems where the transformation deformation gradient can be treated as the thermal deformation gradient with volumetric and shear components. The proposed numerical technique has some common features with known ones for the case without PT [10,11]. The usage of the current configuration and the true Cauchy stresses along with assumptions of small elastic strains and zero modified plastic spin allow us to use—with small modifications—the radial return algorithm and the consistent elastoplastic moduli for the case of small strains [8,14].

When an elastoplastic problem with the radial return algorithm is incrementally solved, usually one integration point (with implicit or explicit scheme) is used for calculation of stresses at the end of a load step, i.e. when the increment of the deformation gradient is known then the stresses are directly calculated through elastoplastic constitutive equations. As the plastic flow rule is formulated in rate form (in contrast to elastic law), then at a large load step (correspondingly a large increment of the deformation gradient) the one point integration can give large deviation from the actual solution. Direct decrease of a load step increases considerably the calculation time. Therefore, we suggest subdividing a known increment of the deformation gradient into a finite number of subincrements and to use the radial return algorithm for subsequent calculations of stresses for all the intermediate values of the deformation gradient up to the final value at the end of a load step. It can be simply implemented and does not essentially increase calculation time because we do not additionally solve the global system of FE equations. Another multipoint integration scheme for small elastoplastic strains was proposed in [15].

In Section 2 the formulation of martensitic PT in elastoplastic materials is described. It includes a concise derivation of PT and twinning criteria from the second law of thermodynamics for material points and transforming volume (nucleus) and description of the complete set of equations. In Section 3 the numerical method with a derivation of the sequence of stress calculation, radial return algorithm (with use of multi integration points within a load increment), finite element scheme and calculation of the consistent tangent moduli are presented. The similarity for the cases of small and large strains are shown. At the end, some numerical examples are solved and analyzed. Appendix A contains the derivation of the rate form of the principle of virtual work for the actual configuration with the Cauchy stress tensor.

Symbolic tensor notations are used throughout this paper. Vectors and tensors are denoted in boldface type;

$\boldsymbol{A}\cdot\boldsymbol{B}$ and $\boldsymbol{A}:\boldsymbol{B}$ are the contraction of tensors over one and two indices. Let a superscripts t and -1 denote transposed and inverse operation; subscripts s and a designate symmetrical and antisymmetrical tensor parts; $\boldsymbol{I}$ is the unit tensor; dev $\boldsymbol{A}$ is a deviatoric part of $\boldsymbol{A}$; $|\boldsymbol{A}|=(\boldsymbol{A}:\boldsymbol{A})^{1/2}$ is the modulus of tensor $\boldsymbol{A}$; $\dot{\boldsymbol{A}}$ is the material time derivative of $\boldsymbol{A}$.

2. Problem formulation at finite strains

Here the martensitic PT will be considered as a special type of deformation of a crystal lattice of parent phase (austenite) into a crystal lattice of product phase (martensite) without diffusion, Figs. 1 and 2(a), which is accompanied by a jump of all the thermomechanical properties. This deformation is called the transformation strain. The transformation deformation gradient cannot be arbitrary (as elastic or plastic strain). For each PT the right stretch transformation tensor is a fixed tensor to within symmetry operations. All intermediate values of the transformation right stretch tensor are unstable and cannot exist in an equilibrium. Due to symmetry there is a finite number (e.g. 12 for PT from a cubic to a monoclinic lattice) of crystallographically equivalent variants of martensite with the same (to within symmetry operations) transformation right stretch tensor.

In the approach considered below, martensitic PT will be described as a growth of the prescribed transformation deformation gradient in some transforming region V_n from the unit tensor to final value which is accompanied by the change of all thermomechanical properties in this region, Fig. 3. Twinning will be described as a particular case of martensitic PT without changing material properties during twin appearance. The transformation strain at twinning has only shear components [16], Fig 2(b).

2.1. Kinematics

Let the motion of the uniformly deformed infinitesimal neighborhood of a material point in a process of martensitic PT be described by the function $\boldsymbol{r}=\boldsymbol{r}(\boldsymbol{r}_\tau, t)$, $t_s\le t\le t_f$, where $\boldsymbol{r}\in V_n$ and $\boldsymbol{r}_\tau\in V_n^\tau$ are the positions of points in the actual V_n and the reference V_n^τ (at $t=0$) configurations, t is the current time, t_s and t_f are the start and finish time of PT in a material point. We neglect thermal strains (they are small with respect to transformation strains) and assume a multiplicative decomposition of the total deformation gradient $\boldsymbol{F}=\partial\boldsymbol{r}/\partial\boldsymbol{r}_\tau$ into elastic $\boldsymbol{F}_e$, transformational $\boldsymbol{F}_t$ and plastic $\boldsymbol{F}_p$ parts [1,2], i.e.

$$\boldsymbol{F}=\boldsymbol{F}_e\cdot\boldsymbol{F}_t\cdot\boldsymbol{F}_p=\boldsymbol{V}_e\cdot\boldsymbol{R}_e\cdot\boldsymbol{F}_t\cdot\boldsymbol{F}_p, \tag{1}$$

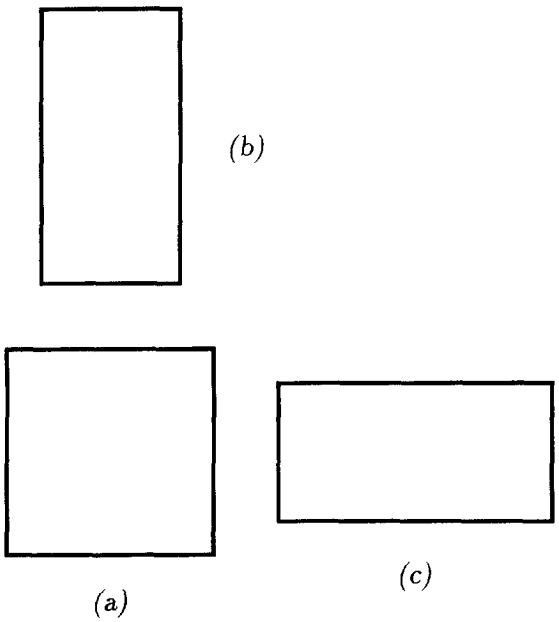

Fig. 1. Scheme of initial crystal lattice (a) and two martensitic variants (b,c).

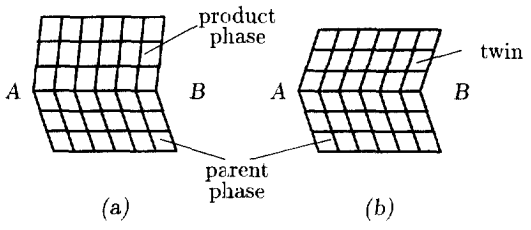

Fig. 2. Deformation due to transformation with invariant plane AB for phase transformation (a) and twinning (b).

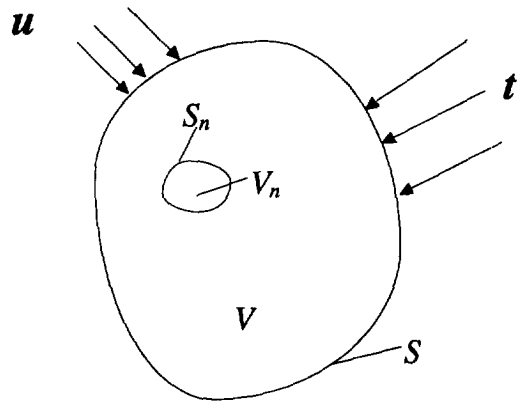

Fig. 3. A sample of volume V with a transforming region V_n and the prescribed traction t and nonzero displacement u at the part of boundary S and zero traction or displacement at the remaining part of S.

where $\boldsymbol{F}_e = \boldsymbol{V}_e \cdot \boldsymbol{R}_e$; $\boldsymbol{V}_e$ is the elastic left stretch (symmetric) tensor, $\boldsymbol{R}_e$ is the elastic rotation tensor. Let us introduce the internal dimensionless time (the order parameter) ξ $(0 \le \xi \le 1)$ which is related to $\boldsymbol{F}_t$ and has the following properties: PT starts at $\xi = 0$ and finishes at $\xi = 1$; when ξ varies between 0 and 1, the transformation deformation gradient grows from $\boldsymbol{I}$ to final maximum value $\bar{\boldsymbol{F}}_t$ determined by crystallography. It is possible to define the order parameter ξ e.g. as $\xi := |\boldsymbol{F}_t - \boldsymbol{I}|/|\bar{\boldsymbol{F}}_t - \boldsymbol{I}|$. Using Eq. (1) the velocity gradient $\boldsymbol{l}$ and deformation rate $\boldsymbol{d}$ are described as follows:

$$\boldsymbol{l} := \frac{\partial \boldsymbol{v}}{\partial \boldsymbol{r}} = \dot{\boldsymbol{F}} \cdot \boldsymbol{F}^{-1} = \dot{\boldsymbol{F}}_e \cdot \boldsymbol{F}_e^{-1} + \boldsymbol{F}_e \cdot \dot{\boldsymbol{F}}_t \cdot \boldsymbol{F}_t^{-1} \cdot \boldsymbol{F}_e^{-1} + \boldsymbol{F}_e \cdot \boldsymbol{F}_t \cdot \dot{\boldsymbol{F}}_p \cdot \boldsymbol{F}_p^{-1} \cdot \boldsymbol{F}_t^{-1} \cdot \boldsymbol{F}_e^{-1}, \tag{2}$$

$$\boldsymbol{d} := (\boldsymbol{l})_s = (\dot{\boldsymbol{F}}_e \cdot \boldsymbol{F}_e^{-1})_s + \boldsymbol{d}_t + \boldsymbol{d}_p, \tag{3}$$

where $\boldsymbol{v} = \dot{\boldsymbol{r}}$ is the velocity vector, $\boldsymbol{d}_t$ and $\boldsymbol{d}_p$ are the rates of the transformational and plastic (due to plastic strain) deformations, respectively (see Box 1). For description of elastic strain we use the elastic strain tensor $\boldsymbol{B}_e$

$$\boldsymbol{B}_e := 0.5(\boldsymbol{F}_e \cdot \boldsymbol{F}_e^{t} - \boldsymbol{I}) = 0.5\,(\boldsymbol{V}_e \cdot \boldsymbol{V}_e - \boldsymbol{I}). \tag{4}$$

We assume that the elastic strains are small, i.e. $\boldsymbol{V}_e = \boldsymbol{I} + \boldsymbol{\varepsilon}_e$, $\boldsymbol{\varepsilon}_e \ll \boldsymbol{I}$, then $\boldsymbol{V}_e^{-1} \approx \boldsymbol{I} - \boldsymbol{\varepsilon}_e$, $\boldsymbol{B}_e \approx \boldsymbol{\varepsilon}_e$. In the approach presented the transformation deformation gradient $\boldsymbol{F}_t$ should be prescribed as input data. For the solution of the PT problem we vary it as

$$\boldsymbol{F}_t = \boldsymbol{I} + \xi\,(\bar{\boldsymbol{F}}_t - \boldsymbol{I}) \quad \xi \in [0,1], \tag{5}$$

where $\bar{\boldsymbol{F}}_t$ is the final value of the transformation deformation gradient at $\xi = 1$.

For a material point without PT we must prescribe in the above presented equations that $\boldsymbol{F}_t = \boldsymbol{I} = \text{const}$ at time $t \le t_s$ or $\boldsymbol{F}_t = \bar{\boldsymbol{F}}_t = \text{const}$ at time $t \ge t_f$.

REMARK 1. To prescribe the final value of the transformation deformation gradient $\bar{\boldsymbol{F}}_t$ we use in this paper the simplest variant of crystallographic theory when the transformation strain results in deformation with invariant (nondeformable and nonrotating) plane, which is called a habit plane [17]. Such a deformation of martensite is compatible with austenite along the habit plane in stress-free state which leads to elastic energy minimization at fine microstructure [18]. In the first approximation the following formula [17] is used

$$\bar{\boldsymbol{F}}_t = \boldsymbol{I} + \boldsymbol{k}\boldsymbol{n}, \tag{6}$$

where $\boldsymbol{n}$ is the outward unit normal vector to the habit plane and $\boldsymbol{k}$ is the displacement vector due to transformation. The tensor $\bar{\boldsymbol{F}}_t$ represents a simple shear along some direction in habit plane and an extension (compression) in orthogonal to habit plane direction. The tensor $\bar{\boldsymbol{F}}_t$ is determined nonuniquely because there are a finite number of possible crystallographic directions of vector $\boldsymbol{n}$ and the corresponding vector $\boldsymbol{k}$ [17] (e.g. there are 24 habit-plane variants for a Fe–30%Ni alloy predicted by crystallographic theory). We consider the

nucleation in some volume where the transformation deformation gradients have the same value in every point of the nucleus (i.e. only one variant from the possible crystallographic ones is realized). Then in order to define a real variant of $\overline{\boldsymbol{F}}_t$ we can check all the possible crystallographic variants of the transformation deformation gradient $\overline{\boldsymbol{F}}_t$ for the transforming region and choose the more favorable one according to the corresponding extremum principle (see below numerical example 4.3). Of course, if we know the directions for the vectors $\boldsymbol{n}$ and $\boldsymbol{k}$ from some other considerations, then we can prescribe the transformation deformation gradient $\overline{\boldsymbol{F}}_t$ uniquely.

REMARK 2. The tensor $\overline{\boldsymbol{F}}_t$ can be represented not always by Eq. (6). For example, for pure dilatational transformation we get

$$\boldsymbol{F}_t = a\boldsymbol{I}\,, \tag{7}$$

where a is a known scalar parameter. In general case from crystallography we can define only components of the transformation right stretch tensor (symmetric) $\overline{\boldsymbol{U}}_t$ ($\overline{\boldsymbol{F}}_t = \boldsymbol{R}_t \cdot \overline{\boldsymbol{U}}_t$). But problem solution does not depend on the transformation rotation tensor $\boldsymbol{R}_t$ because we can combine the rotation tensors $\boldsymbol{R}_t$ and $\boldsymbol{R}_e$ in the total gradient decomposition (1) into one rotation tensor $\boldsymbol{R}_{et} = \boldsymbol{R}_e \cdot \boldsymbol{R}_t$. Therefore, for the sake of convenience, we can also prescribe the transformation deformation gradient with arbitrary rotation tensor $\boldsymbol{R}_t$. There exists a finite number k of variants for admissible transformation right stretch tensors $\overline{\boldsymbol{U}}_t^i$ at $\xi = 1$ where $i = 1, 2, \ldots, k$ and i corresponds to the ith martensitic variant. All $\overline{\boldsymbol{U}}_t^i$ are symmetry-related. Some examples of $\overline{\boldsymbol{U}}_t^1$ for tetragonal, trigonal, orthorhombic and monoclinic martensite are given in [19]. Tensors $\overline{\boldsymbol{U}}_t^i$ for $i > 1$ may be obtained from $\overline{\boldsymbol{U}}_t^1$ by permutating the basis. To choose the actual variant $\overline{\boldsymbol{U}}_t^i$ from all the possible ones we have to use the corresponding extremum principle (the same as for the choice of the actual variant of $\overline{\boldsymbol{F}}_t$ with a habit plane, see Remark 1).

REMARK 3. As an idealization we can consider not a finite but an infinite number of variants for the tensor $\overline{\boldsymbol{F}}_t$ which differ one from another by an arbitrary rotation tensor $\boldsymbol{R}_o$, i.e. any variant i of $\overline{\boldsymbol{F}}_t$ reads as follows

$$\boldsymbol{F}_t^i = \boldsymbol{R}_o^1 : \overline{\boldsymbol{F}}_t : \boldsymbol{R}_o, \tag{8}$$

where $\overline{\boldsymbol{F}}_t$ is fixed and prescribed by Eq. (6). To find the actual variant of $\overline{\boldsymbol{F}}_t^i$ or the tensor $\boldsymbol{R}_o$ the extremum principle (the same as for choosing a favorable variant from a finite number of variants) should be used.

2.2. Thermodynamical aspects of PT for material point

Here, we briefly present the approach for description of PT suggested in [1,2]. All equations will be written in the actual configuration. We consider simple materials only, i.e. the response of material in a given point is independent of thermomechanical parameters in other points.

We use the second law of thermodynamics in the form of the local Planck inequality

$$\rho\mathscr{D} = \boldsymbol{T} : \boldsymbol{d} - \rho\dot{\psi} - \rho s\dot{\theta} \geq 0. \tag{9}$$

Here, $\mathscr{D}$ is the rate of dissipation per unit mass, $\boldsymbol{T}$ is the Cauchy stress tensor, s is the specific entropy, θ is the temperature, ψ is the specific (per unit mass) Helmholtz free energy, ρ is the mass density. We assume that

$$\psi = \psi(\boldsymbol{B}_e, \theta, \xi). \tag{10}$$

Then, differentiating Eq. (10) and inserting the result in expression (9) along with Eqs. (3), (5) and $(18)_1$ we get

$$\mathscr{D} = \left(\frac{1}{\rho}\boldsymbol{T} : (\dot{\boldsymbol{F}}_e \cdot \boldsymbol{F}_e^{-1})_s - \frac{\partial\psi}{\partial\boldsymbol{B}_e} : \dot{\boldsymbol{B}}_e\right) + \frac{1}{\rho}\boldsymbol{T} : \boldsymbol{d}_p - \left(\frac{\partial\psi}{\partial\theta} + s\right)\dot{\theta}$$
$$+ \left(\frac{1}{\rho}\boldsymbol{T} : (\boldsymbol{F}_e \cdot \overline{\boldsymbol{F}}_t \cdot \boldsymbol{F}_t^{-1} \cdot \boldsymbol{F}_e^{-1})_s - \frac{\partial\psi}{\partial\xi}\right)\dot{\xi} \geq 0. \tag{11}$$

Using direct calculations it is possible to show [20] that

$$\left(\frac{1}{\rho}\boldsymbol{T} : (\dot{\boldsymbol{F}}_e \cdot \boldsymbol{F}_e^{-1})_s - \frac{\partial\psi}{\partial\boldsymbol{B}_e} : \boldsymbol{B}_e\right) = \left(\frac{1}{\rho}\boldsymbol{V}_e^{-1} \cdot \boldsymbol{T} \cdot \boldsymbol{V}_e^{-1} - \frac{\partial\psi}{\partial\boldsymbol{B}_e}\right) : \mathring{\boldsymbol{B}}_e, \tag{12}$$

where $\mathring{\boldsymbol{B}}_e := \dot{\boldsymbol{B}}_e + \boldsymbol{B}_e \cdot \boldsymbol{\Omega} + \boldsymbol{\Omega}^t \cdot \boldsymbol{B}_e$ is called the R-derivative associated with the skew-symmetric spin tensor $\boldsymbol{\Omega} = \dot{\boldsymbol{R}}_e \cdot \boldsymbol{R}_e^t$.

Box 1.
Problem formulation

1. *Kinematics*

Multiplicative decomposition of the total deformation gradient $\boldsymbol{F}$

$$\boldsymbol{F} = \frac{\partial \boldsymbol{r}}{\partial \boldsymbol{r}_\tau} = \boldsymbol{F}_e \cdot \boldsymbol{F}_t \cdot \boldsymbol{F}_p = \boldsymbol{V}_e \cdot \boldsymbol{R}_e \cdot \boldsymbol{F}_t \cdot \boldsymbol{F}_p. \tag{13}$$

The elastic strain tensor $\boldsymbol{B}_e$ and the internal dimensionless time ξ

$$\boldsymbol{B}_e := 0.5(\boldsymbol{F}_e \cdot \boldsymbol{F}_e^t - \boldsymbol{I}) = 0.5(\boldsymbol{V}_e \cdot \boldsymbol{V}_e - \boldsymbol{I}), \qquad \xi := \frac{|\boldsymbol{F}_t - \boldsymbol{I}|}{|\bar{\boldsymbol{F}}_t - \boldsymbol{I}|}. \tag{14}$$

The transformation gradient $\boldsymbol{F}_t$

$$\boldsymbol{F}_t = \boldsymbol{I} + \xi(\bar{\boldsymbol{F}}_t - \boldsymbol{I}), \qquad \xi \in [0,1]. \tag{15}$$

Decomposition of the total deformation rate $\boldsymbol{d}$

$$\boldsymbol{d} := (\frac{\partial \boldsymbol{v}}{\partial \boldsymbol{r}})_s = (\dot{\boldsymbol{F}}_e \cdot \boldsymbol{F}_e^{-1})_s + \boldsymbol{d}_t + \boldsymbol{d}_p, \tag{16}$$

$$\boldsymbol{d}_p := (\boldsymbol{F}_e \cdot \boldsymbol{F}_t \cdot \dot{\boldsymbol{F}}_p \cdot \boldsymbol{F}_p^{-1} \cdot \boldsymbol{F}_t^{-1} \cdot \boldsymbol{F}_e^{-1})_s = \boldsymbol{F}_e \cdot \boldsymbol{F}_t \cdot \dot{\boldsymbol{F}}_p \cdot \boldsymbol{F}_p^{-1} \cdot \boldsymbol{F}_t^{-1} \cdot \boldsymbol{F}_e^{-1}, \tag{17}$$

$$\boldsymbol{d}_t := (\boldsymbol{F}_e \cdot \dot{\boldsymbol{F}}_t \cdot \boldsymbol{F}_t^{-1} \cdot \boldsymbol{F}_e^{-1})_s = (\boldsymbol{F}_e \cdot \bar{\boldsymbol{F}}_t \cdot \boldsymbol{F}_t^{-1} \cdot \boldsymbol{F}_e^{-1})_s \dot{\xi}, \qquad \dot{q} := (2/3 \boldsymbol{d}_p : \boldsymbol{d}_p)^{1/2}. \tag{18}$$

2. *Constitutive equations*

Elastic Hooke's law $\boldsymbol{T} = \boldsymbol{E}(\xi) : \boldsymbol{B}_e = K(\xi) I_1(\boldsymbol{B}_e) \boldsymbol{I} + 2G(\xi) \operatorname{dev} \boldsymbol{B}_e$. (19)

Yield function $f(\boldsymbol{T}, q, \xi) = \sigma_i - \sigma_y(q, \xi) \le 0$. (20)

Plastic flow rule $\boldsymbol{d}_p = \lambda \boldsymbol{s}$. (21)

The Kuhn–Tucker conditions $f(\boldsymbol{T}, q, \xi) \le 0, \quad \lambda \ge 0, \quad \lambda f(\boldsymbol{T}, q, \xi) = 0$. (22)

3. *Equilibrium equations* (with body forces $\boldsymbol{f}$) $\nabla \cdot \boldsymbol{T} + \rho \boldsymbol{f} = 0$.

4. (a) *PT criterion*

$$\bar{X} := \frac{1}{m_n} \int_{V_n} \int_0^1 \boldsymbol{T} : \boldsymbol{d}_t \frac{\mathrm{d}t}{\mathrm{d}\xi} \mathrm{d}\xi \, \mathrm{d}V_n - (\psi_2^\theta - \psi_1^\theta) = k_c, \qquad m_n = \int_{V_n} \rho \, \mathrm{d}V_n. \tag{23}$$

(b) *Twinning criterion*

$$\bar{X} := \varphi = k_c, \qquad \varphi := \frac{1}{m_n} \int_{V_n} \int_0^1 \boldsymbol{T} : \boldsymbol{d}_t \frac{\mathrm{d}t}{\mathrm{d}\xi} \mathrm{d}\xi \, \mathrm{d}V_n. \tag{24}$$

5. *Extremum principle for PT with test function* $V_n^\diamond$, $\bar{\boldsymbol{F}}_t^\diamond$

$$\bar{X}(V_n^\diamond, \bar{\boldsymbol{F}}_t^\diamond) - k_c < 0 = \bar{X}(V_n, \bar{\boldsymbol{F}}_t) - k_c \qquad \text{or} \qquad \varphi(V_n, \bar{\boldsymbol{F}}_t) \to \max. \tag{25}$$

The assumption that the rate of dissipation D is independent of $\mathring{\boldsymbol{B}}_e$ and $\dot{\theta}$ results in the hyperelasticity law and expression for entropy, as well as in a reduced dissipative inequality:

$$\boldsymbol{T} = \rho \boldsymbol{V}_e \cdot \frac{\partial \psi}{\partial \boldsymbol{B}_e} \cdot \boldsymbol{V}_e; \qquad s = -\frac{\partial \psi}{\partial \theta}; \tag{26}$$

$$\mathscr{D} = \frac{1}{\rho} \boldsymbol{T} : \boldsymbol{d}_p + X_\xi \dot{\xi} \geq 0, \tag{27}$$

where

$$X_\xi = \frac{1}{\rho} \boldsymbol{T} : (\boldsymbol{F}_e \cdot \bar{\boldsymbol{F}}_t \cdot \boldsymbol{F}_t^{-1} \cdot \boldsymbol{F}_e^{-1})_s - \frac{\partial \psi}{\partial \xi} \tag{28}$$

is the dissipative force conjugated to dissipative rate $\dot{\xi}$. The simplest assumption that each rate depends on the conjugate force only leads to evolution equations

$$\boldsymbol{d}_p = \boldsymbol{f}_p(\boldsymbol{T}); \qquad \dot{\xi} = f_\xi(X_\xi). \tag{29}$$

Eq. $(29)_1$ is the flow rule and Eq. $(29)_2$ is the kinetic equation for PT. The allowance for mutual influence of all thermomechanical processes can be made in a standard way.

We assume that the condition $\dot{\xi}=0$ is valid at $X_\xi=0$ only. Then it is possible to describe the equilibrium PT ($\dot{\xi}\to 0$) with the equation $X_\xi=0$ (see Eq. (28)). This is one scalar equation and it is always possible for each ξ and $\theta(\xi)$ to choose six components of stress tensor $\boldsymbol{T}(\xi, \theta(\xi))$ to satisfy this equation. If the actual stress variation follows this dependence, then the phase equilibrium is possible for arbitrary ξ. But from the experiments it follows that the phase equilibrium is impossible at $0<\xi<1$, only at $\xi=0$ and $\xi=1$ do we have the stable equilibrium. At $0<\xi<1$ a nonequilibrium process takes place, which requires energy and stress fluctuations.

In order to overcome this contradiction we will use average description over a PT duration $t_p=t_f-t_s$ suggested in [1,2]. We introduce the averaged dissipation rate due to PT

$$\mathscr{D}_\xi := \frac{1}{t_p} \int_0^{t_p} X_\xi \dot{\xi} \, dt = \frac{1}{t_p} \int_0^1 X_\xi \, d\xi = \frac{X}{t_p} = X\dot{\chi}, \tag{30}$$

where

$$X := \int_0^1 X_\xi \, d\xi, \qquad \dot{\chi} := \frac{1}{t_p} \tag{31}$$

are the averaged dissipative force and rate. The definition of dissipative rate is logical, because a variation of the parameter ξ during the time t_p is one. The dissipative force is defined as a conjugate variable in the expression for the rate of dissipation. In order to describe PT with dissipation and hysteresis (i.e. direct and reverse PT begin at different values X and between these values PT is impossible) the following criterion for a material point was suggested in [1,2]

$$X = k_c, \tag{32}$$

where k_c is the threshold value of dissipation X due to PT which is experimentally determined and can depend on some parameters, for example θ, $\boldsymbol{F}_p$.

In this paper we will consider isothermal PT, i.e. $\dot{\theta}=0, \nabla\theta=0$. Then from Eqs. (9) and (27) it follows that

$$X_\xi \dot{\xi} = \frac{1}{\rho} \boldsymbol{T} : (\boldsymbol{d} - \boldsymbol{d}_p) - \dot{\psi}. \tag{33}$$

Allowing for Eqs. (30) and (32) we get

$$X := \int_0^1 \frac{1}{\rho} \boldsymbol{T} : \boldsymbol{d} \frac{dt}{d\xi} \, d\xi - \int_0^1 \frac{1}{\rho} \boldsymbol{T} : \boldsymbol{d}_p \frac{dt}{d\xi} \, d\xi - (\psi_2 - \psi_1) = k_c, \tag{34}$$

where ψ_2, ψ_1 are the specific Helmholtz free energies for the second (after PT) and the first (before PT) phase, $\rho=\rho(\xi)=\det(\boldsymbol{F}(\xi))\rho_1$ is the mass density during PT, ρ_1 is the mass density at $\xi=0$, i.e. before PT.

REMARK. We use assumption that the temperature can be homogeneously changed in a sample before or after PT in some volume, but is fixed during PT.

2.3. Constitutive equations

We use the generalization of the Prandtl–Reuss equations to the case of large strains for isotropic elastoplastic materials with isotropic hardening. The relationships during PT are presented in Box 1. Here, q is the accumulated plastic strain; $\sigma_i=(3/2\boldsymbol{s}:\boldsymbol{s})^{1/2}$ is the stress intensity; $\boldsymbol{s}=\operatorname{dev}\boldsymbol{T}$ is the deviatoric Cauchy stress tensor; $\sigma_y(q,\xi)$ is the yield stress, a function to be found experimentally; $\boldsymbol{E}(\xi)$ is the elastic modulus tensor; $K(\xi)$, $G(\xi)$ are the elastic coefficients which depend on ξ; $I_1(\boldsymbol{B}_e)=\boldsymbol{I}:\boldsymbol{B}_e$ is the first invariant of $\boldsymbol{B}_e$. It is necessary to make some remarks.

(1) From Eq. $(26)_1$ for small elastic strains we get $T=\rho(\partial\psi)/(\partial\boldsymbol{B}_e)$. We assume that

$$\psi(B_e,\theta,\xi)=\frac{\boldsymbol{B}_e:\boldsymbol{E}(\xi):\boldsymbol{B}_e}{2\rho(\xi)}+\psi^{\theta}(\theta,\xi), \tag{35}$$

where ψ^{θ} is the thermal part of the specific Helmholtz free energy (a function of temperature only). Then we get Hooke's law (19).

(2) To get a unique decomposition of the total deformation gradient into elastic and plastic parts we assume that the modified plastic spin is zero, i.e.

$$(\boldsymbol{F}_e\cdot\boldsymbol{F}_t\cdot\dot{\boldsymbol{F}}_p\cdot\boldsymbol{F}_p^{-1}\cdot\boldsymbol{F}_t^{-1}\cdot\boldsymbol{F}_e^{-1})_a=\boldsymbol{0}. \tag{36}$$

Similar assumption is accepted in many papers on large strains without PT, see for example [10,11]. It allows us to determine the rate of plastic deformation gradient $\dot{\boldsymbol{F}}_p$ through the rate of plastic deformation $\boldsymbol{d}_p$ (see below).

(3) The plastic flow rule (21) is a particular case of Eq. $(29)_1$. In our first papers on PT simulations at finite strains [12,13] we have used in Eqs. (13) and (17) the symmetric plastic deformation gradient $\boldsymbol{U}_p$ with 6 components instead of $\boldsymbol{F}_p$ with 9 components as here. Therefore, we did not need additional equations like Eq. (36) (3 equations in a component form). But the final equations in [12,13] are more complicated for calculations as we have to use objective derivatives in numerical scheme.

2.4. Nucleation criterion

Assume that in some volume V_n with the boundary S_n fixed relative to the material's points, due to PT during the time Δt, the new nuclei appeared, i.e. some material mass m_n undergoes the PT.

As shown in [1,2] we have to average PT criterion (32) over the transforming region, similar to averaging over the transformation time. Condition of *nucleation* looks as [1,2]

$$\int_{m_n} X\,\mathrm{d}m_n=\int_{m_n} k_c\,\mathrm{d}m_n. \tag{37}$$

Using Eq. (34) we get

$$\int_{V_n} X\,\mathrm{d}V_n:=\int_{V_n}\int_0^1\frac{\rho_1}{\rho(\xi)}\boldsymbol{T}:\boldsymbol{d}\,\frac{\mathrm{d}t}{\mathrm{d}\xi}\,\mathrm{d}\xi\,\mathrm{d}V_n-\int_{V_n}\int_0^1\frac{\rho_1}{\rho(\xi)}\boldsymbol{T}:\boldsymbol{d}_p\,\frac{\mathrm{d}t}{\mathrm{d}\xi}\,\mathrm{d}\xi\,\mathrm{d}V_n-\int_{V_n}\rho_1(\psi_2-\psi_1)\,\mathrm{d}V_n=\int_{V_n}\rho_1 k_c\,\mathrm{d}V_n, \tag{38}$$

where X is the local dissipation increment in the course of PT due to PT only (excluding plastic and other types of dissipation, see Section 2.2), $\int_{V_n}\int_0^1(\rho_1/\rho(\xi))\boldsymbol{T}:\boldsymbol{d}_p\,\mathrm{d}\xi\,\mathrm{d}V_n$ is the total dissipation increment in the course of PT due to plastic deformation only, V_n is the volume of nucleus at $\xi=0$ (before PT). It is necessary to note that we will not require fulfillment of the condition (32) in every point of nucleus.

We use the following simplifications of Eq. (38):

(a) the phases have the same elastic properties $\boldsymbol{E}(\xi)=\boldsymbol{E}_1=\boldsymbol{E}_2=\text{const}$;

(b) $\rho(\xi)\approx\rho=\text{const}$, i.e. volumetric transformation strain is small in comparison with the unit (elastic strains are small, plastic strains due to incompressibility do not change mass density, see below Section 3.1);

(c) θ and k_c are homogeneous in the nucleus.

Then, Eq. (38) can be transformed into Eq. (23), where $\bar{X}$ is the driving force for nucleation (averaged over the nucleus value of X), m_n is the nucleus mass. Here we take into account Eqs. (12), (16), $(26)_1$, (35) and

$$\int_0^1 \boldsymbol{T}:(\dot{\boldsymbol{F}}_e\cdot\boldsymbol{F}_e^{-1})_s\frac{dt}{d\xi}d\xi=\int_0^1 \boldsymbol{T}:\mathring{\boldsymbol{B}}_e\frac{dt}{d\xi}d\xi=\int_0^1 \boldsymbol{T}:\dot{\boldsymbol{B}}_e\frac{dt}{d\xi}d\xi=\int_0^1 \boldsymbol{B}_e:\boldsymbol{E}:\dot{\boldsymbol{B}}_e\frac{dt}{d\xi}d\xi=\frac{\boldsymbol{B}_e^2:\boldsymbol{E}:\boldsymbol{B}_e^2}{2}-\frac{\boldsymbol{B}_e^1:\boldsymbol{E}:\boldsymbol{B}_e^1}{2}, \tag{39}$$

where $\boldsymbol{B}_e^2$ and $\boldsymbol{B}_e^1$ are the elastic strain in a material point after and before PT respectively. Eq. (23) is a final form of the PT criterion which is used in the present paper.

The explicit expressions for ψ^θ can be adopted in the following form [21]

$$\begin{aligned}\psi_1^\theta&=\psi_{o1}-s_{o1}(\theta-\theta_o)-\nu_1\theta\left(\ln\frac{\theta}{\theta_o}-1\right)-\nu_1\theta_o,\\ \psi_2^\theta&=\psi_{o2}-s_{o2}(\theta-\theta_o)-\nu_2\theta\left(\ln\frac{\theta}{\theta_o}-1\right)-\nu_2\theta_o.\end{aligned} \tag{40}$$

Here, $\nu_1>0$ and $\nu_2>0$ are specific heats, s_{o1}, s_{o2}, ψ_{o1}, ψ_{o2} are constants, θ_o is a reference temperature.

Using the presented thermomechanical approach twinning can be described as a particular case of martensitic PT, i.e. material properties of a parent phase and a twin are the same, but during twin appearance the additional transformation deformation gradient in a twin (like for martensitic PT) is induced [2]. Therefore criterion for twin appearance looks like Eq. (24) because the thermal parts of the specific Helmholtz free energy for both phases are the same $\psi_1^\theta=\psi_2^\theta$.

2.5. Extremum principle for PT

In the general case, position, shape, volume V_n of the new nucleus (transforming region) and the actual variant of the transformation deformation gradient $\overline{\boldsymbol{F}}_t$ (in PT criterion (38) or (23) for each increment of boundary conditions or temperature θ) are unknown. To determine them, we can use extremum principle $(25)_1$ which follows from the postulate of realizability [22], where the superscript $\diamond$ designates the possible admitted quantities (the actual values are designated without this superscript). The physical interpretation of principle $(25)_1$ is as follows: as soon as for some region V_n and the variant $\overline{\boldsymbol{F}}_t$ of the transformation deformation gradient the PT criterion (23) is fulfilled for the first time, PT occurs in V_n with the $\overline{\boldsymbol{F}}_t$. For all other $V_n^\diamond$ and $\overline{\boldsymbol{F}}_t^\diamond$ inequality $(25)_1$ is valid, because in the opposite case PT criterion (23) will be met for this $V_n^\diamond$ and $\overline{\boldsymbol{F}}_t^\diamond$ earlier than for V_n and $\overline{\boldsymbol{F}}_t$. As only the work integral φ in Eq. $(25)_1$ depends on the volume V_n and the transformation deformation gradient $\overline{\boldsymbol{F}}_t$, the extremum principle $(25)_2$ follows from the principle $(25)_1$.

For more general case when PT criterion (38) is used the extremum principle has the following form [2]

$$\begin{aligned}&\int_{V_n}\int_0^1\frac{\rho_1}{\rho(\xi)}\boldsymbol{T}:\boldsymbol{d}\frac{dt}{d\xi}d\xi\,dV_n-\int_{V_n}\int_0^1\frac{\rho_1}{\rho(\xi)}\boldsymbol{T}:\boldsymbol{d}_p\frac{dt}{d\xi}d\xi\,dV_n-\int_{V_n}\rho_1(\psi_2-\psi_1)\,dV_n-\int_{V_n}\rho_1 k_c\,dV_n=0\\ &>\int_{V_n^\diamond}\int_0^1\frac{\rho_1^\diamond}{\rho^\diamond(\xi)}\boldsymbol{T}^\diamond:\boldsymbol{d}^\diamond\frac{dt}{d\xi}d\xi\,dV_n-\int_{V_n^\diamond}\int_0^1\frac{\rho_1^\diamond}{\rho^\diamond(\xi)}\boldsymbol{T}^\diamond:\boldsymbol{d}_p^\diamond\frac{dt}{d\xi}d\xi\,dV_n-\int_{V_n^\diamond}\rho_1^\diamond(\psi_2^\diamond-\psi_1)\,dV_n-\int_{V_n^\diamond}\rho_1^\diamond k_c^\diamond\,dV_n.\end{aligned} \tag{41}$$

The problem formulation presented in Box 1 must be completed by the standard boundary conditions.

3. Numerical method

In this paper we consider the 'inverse' problem, i.e. at some variation of temperature or (and) boundary conditions (we call it by variation of generalized external load P, Fig. 4(a)) a new nucleus appears in the body, and we assume in advance the position and size of the transforming region (nucleus). The temperature during PT is assumed to be fixed. Then, the condition for PT will be defined from the PT criterion (23). For example, when stress–strain state and φ are computed we can determine the temperature of PT from Eq. (23). This is a scalar equation with respect to temperature. Extremum principle in the form Eq. $(25)_2$ is used to analyze the solutions obtained. In order to calculate variation of stress–strain state during PT as a function of the growing transformation deformation gradient we have to solve incrementally elastoplastic problem with the prescribed transformation deformation gradient $\boldsymbol{F}_t$ in the region where PT is assumed to occur. This formulation is kinematically similar to the problem of thermoplasticity [23], i.e. the order parameter ξ can be treated like the temperature and the transformation deformation gradient like the thermal deformation gradient (anisotropic thermal expansion). Below, we describe the solution algorithm for PT in the elastoplastic problem at finite strains which has some common features with known ones for the case without PT [10,11]. The algorithm can be modified from the case of small strains to finite ones.

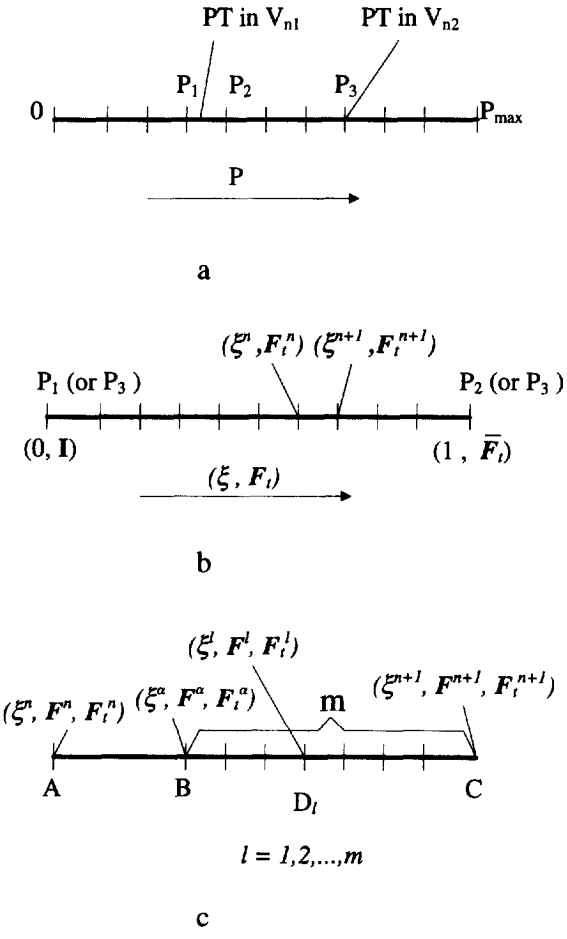

Fig. 4. Schematic description of change of generalized external load P (a), the order parameter ξ and the transformation deformation gradient $\boldsymbol{F}_t$ (b), subdivision of the deformation gradient $\boldsymbol{F}$, the transformation deformation gradient $\boldsymbol{F}_t$ and the order parameter ξ within a load increment at numerical integration (c).

3.1. Stress calculation

The solution is realized in step-by-step form, i.e. with a known solution at time t_n one should find a solution at time t_{n+1}, where n is a load step number. It is necessary to note that PT in transforming region V_n (Fig. 3) can occur at fixed (e.g. at fixed generalized external load P_3, Fig. 4(a)) or changing boundary conditions (e.g. at changing generalized external load from P_1 to P_2, Fig. 4(a)). A load increment for PT in some region V_n corresponds to a small change of the order parameter from ξ^n to ξ^{n+1} $(0 \le \xi \le 1)$ and to the change of the transformation deformation gradient $\boldsymbol{F}_t^{n+1}$ and, if necessary, to the boundary conditions corresponding to this variation of ξ, Fig. 4(b). At deformation without PT a load increment is a small change of the boundary conditions and temperature. Calculations are carried out in the current configuration using the true Cauchy stress tensor. First let us consider integration procedure at elastoplastic deformation, i.e. how one can calculate stresses through the known values of the total $\boldsymbol{F}^{n+1}$ and transformation $\boldsymbol{F}_t^{n+1}$ deformation gradients and the order ξ^{n+1} at the end of a load step (at time t_{n+1}). From Eqs. (17) and (21) we get

$$\dot{\boldsymbol{F}}_p \cdot \boldsymbol{F}_p^{-1} = \lambda \boldsymbol{F}_{et}^{-1} \cdot \boldsymbol{s} \cdot \boldsymbol{F}_{et}, \tag{42}$$

where $\boldsymbol{F}_{et} = \boldsymbol{F}_e \cdot \boldsymbol{F}_t$. Then, the plastic deformation gradient $\boldsymbol{F}_p$ is integrated by means of the exponential formula [10]

$$\boldsymbol{F}_p^{n+1} = \exp(\lambda (\boldsymbol{F}_{et}^{n+1})^{-1} \cdot \boldsymbol{s}^{n+1} \cdot \boldsymbol{F}_{et}^{n+1}) \cdot \boldsymbol{F}_p^n = (\boldsymbol{F}_{et}^{n+1})^{-1} \cdot \exp(\lambda \boldsymbol{s}^{n+1}) \cdot \boldsymbol{F}_{et}^{n+1} \cdot \boldsymbol{F}_p^n. \tag{43}$$

Equality $(43)_3$ can be checked using definition of the exponential function. Plastic incompressibility is exactly represented by the approximation Eq. (43), because

$$\det(\boldsymbol{F}_p^{n+1}) = \det(\boldsymbol{F}_{et}^{n+1})^{-1} \det[\exp(\lambda \boldsymbol{s}^{n+1})] \det(\boldsymbol{F}_{et}^{n+1}) \det(\boldsymbol{F}_p^n) = \det(\boldsymbol{F}_p^n) = 1 \tag{44}$$

due to $\det[\exp(\lambda \boldsymbol{s}^{n+1})] = \exp(\boldsymbol{I} : \lambda \boldsymbol{s}^{n+1}) = \exp(0) = 1$, see also [10].

For the trial elastic predictor we can write

$$\boldsymbol{F}^{n+1} = \boldsymbol{F}_{et}^* \cdot \boldsymbol{F}_p^n, \qquad \boldsymbol{F}_{et}^* := \boldsymbol{F}_e^* \cdot \boldsymbol{F}_t^{n+1}, \tag{45}$$

where $\boldsymbol{F}_e^*$ is a 'trial value' of the elastic deformation gradient. At elastoplastic deformation from Eq. (43) it follows that

$$\boldsymbol{F}^{n+1} = \boldsymbol{F}_{et}^{n+1} \cdot \boldsymbol{F}_p^{n+1} = \boldsymbol{F}_{et}^{n+1} \cdot \boldsymbol{F}_{et}^{(n+1)-1} \cdot \exp(\lambda \boldsymbol{s}^{n+1}) \cdot \boldsymbol{F}_{et}^{n+1} \cdot \boldsymbol{F}_p^n = \exp(\lambda \boldsymbol{s}^{n+1}) \cdot \boldsymbol{F}_{et}^{n+1} \cdot \boldsymbol{F}_p^n. \tag{46}$$

Then, from Eqs. (45) and (46) we obtain

$$\boldsymbol{F}_{et}^* = \boldsymbol{V}_e^* \cdot \boldsymbol{R}_e^* \cdot \boldsymbol{F}_t^{n+1} = \boldsymbol{F}^{n+1} \cdot \boldsymbol{F}_p^{(n)-1} = \exp(\lambda \boldsymbol{s}^{n+1}) \cdot \boldsymbol{F}_{et}^{n+1} = \exp(\lambda \boldsymbol{s}^{n+1}) \cdot \boldsymbol{V}_e^{n+1} \cdot \boldsymbol{R}_e^{n+1} \cdot \boldsymbol{F}_t^{n+1}, \tag{47}$$

and hence

$$\boldsymbol{V}_e^* \cdot \boldsymbol{R}_e^* = \exp(\lambda \boldsymbol{s}^{n+1}) \cdot \boldsymbol{V}_e^{n+1} \cdot \boldsymbol{R}_e^{n+1}. \tag{48}$$

Due to the isotropic elastic law (19) the symmetrical tensors $\exp(\lambda \boldsymbol{s}^{n+1})$ and $\boldsymbol{V}_e^{n+1}$ have the same principal directions, and therefore their product is a symmetric tensor. Then, because of the uniqueness of the polar decomposition, Eq. (48) yields

$$\boldsymbol{V}_e^* = \exp(\lambda \boldsymbol{s}^{n+1}) \cdot \boldsymbol{V}_e^{n+1}, \tag{49}$$

$$\boldsymbol{R}_e^* = \boldsymbol{R}_e^{n+1}. \tag{50}$$

Taking the logarithm of both sides of Eq. (49), we get

$$\ln \boldsymbol{V}_e^* = \lambda \boldsymbol{s}^{n+1} + \ln \boldsymbol{V}_e^{n+1}. \tag{51}$$

As elastic strains are small $\boldsymbol{V}_e^{n+1} = \boldsymbol{I} + \boldsymbol{\varepsilon}_e^{n+1}$, $\boldsymbol{\varepsilon}_e^{n+1} \ll \boldsymbol{I}$ then $\ln \boldsymbol{V}_e^{n+1} = \boldsymbol{\varepsilon}_e^{n+1}$. Let us designate $\ln \boldsymbol{V}_e^* = \boldsymbol{\varepsilon}_e^*$, where $\boldsymbol{\varepsilon}_e^*$ generally is not small. Then

$$\boldsymbol{\varepsilon}_e^{n+1} = \boldsymbol{\varepsilon}_e^* - \lambda \boldsymbol{s}^{n+1}. \tag{52}$$

Eq. (52), the elasticity law Eq. (19) and the flow plastic rule (21) have the same form as for the case of small strains. Therefore in calculating stresses we can use directly the radial return algorithm [8,14], Box 2.

Box 2.
The radial return algorithm

1. Compute trial elastic strain $\boldsymbol{\varepsilon}_e^*$

$$\boldsymbol{F}_e^* = \boldsymbol{F}^{n+1} \cdot (\boldsymbol{F}_p^n)^{-1} \cdot (\boldsymbol{F}_t^{n+1})^{-1}, \tag{53}$$

$$\boldsymbol{\varepsilon}_e^* = \ln \boldsymbol{V}_e^* = \frac{1}{2} \ln(\boldsymbol{V}_e^* \cdot \boldsymbol{V}_e^*) = \frac{1}{2} \ln[\boldsymbol{F}_e^* \cdot (\boldsymbol{F}_e^*)^t]. \tag{54}$$

2. Compute trial elastic deviatoric stress s^*

$$\boldsymbol{s}^* = 2G \operatorname{dev} \boldsymbol{\varepsilon}_e^*.$$
$$\text{If } |\boldsymbol{s}^*| - \sqrt{\frac{2}{3}}\, \sigma_y(q^n, \xi^{n+1}) \le 0 \quad \text{then} \quad \boldsymbol{s}^{n+1} = \boldsymbol{s}^* \quad \text{and go to 6.} \tag{55}$$

3. Compute unit normal field $\bar{\boldsymbol{n}}$

$$\bar{\boldsymbol{n}} = \frac{\boldsymbol{s}^*}{|\boldsymbol{s}^*|}. \tag{56}$$

4. Compute consistency parameter λ by local iterations from the following nonlinear algebraic equation

$$|\boldsymbol{s}^*| - 2G\lambda = \sqrt{\frac{2}{3}}\, \sigma_y\left(q^n + \sqrt{\frac{2}{3}}\, \lambda, \xi^{n+1}\right). \tag{57}$$

5. Compute the equivalent plastic strain q^{n+1}, plastic deformation gradient $\boldsymbol{F}_p^{n+1}$ and deviatoric stress $\boldsymbol{s}^{n+1}$

$$q^{n+1} = q^n + \sqrt{\frac{2}{3}}\, \lambda, \tag{58}$$

$$\boldsymbol{s}^{n+1} = \sqrt{\frac{2}{3}}\, \sigma_y(q^{n+1}, \xi^{n+1}) \bar{\boldsymbol{n}}, \tag{59}$$

$$\boldsymbol{F}_p^{n+1} = (\boldsymbol{F}_t^{(n+1)})^{-1} \cdot (\boldsymbol{F}_e^*)^{-1} \cdot \exp(\lambda \boldsymbol{s}^{n+1}) \cdot \boldsymbol{F}_e^* \cdot \boldsymbol{F}_t^{n+1} \cdot \boldsymbol{F}_p^n. \tag{60}$$

6. Add the mean stress (due to elastic volume change)

$$T^{n+1} = \boldsymbol{s}^{n+1} + K(\boldsymbol{\varepsilon}_e^* : \boldsymbol{I})\boldsymbol{I}. \tag{61}$$

In contrast to the radial return algorithm for the case of small strains we add only the calculation of some kinematic parameters, namely $\boldsymbol{F}_e^*$ and $\boldsymbol{\varepsilon}_e^*$ (Step 1, Box 2) and $\boldsymbol{F}_p^{n+1}$ (Step 5, Box 2).

Let us consider the use of the radial return algorithm for large load increments. In this case it can give a large deviation from the exact continuous solution due to only one point for integration of constitutive equations per time step, Eq. (43) (or when explicit or implicit scheme is used for a derivative approximation). Therefore we suggest to use numerical integration of constitutive equations with a finite number of intermediate integration

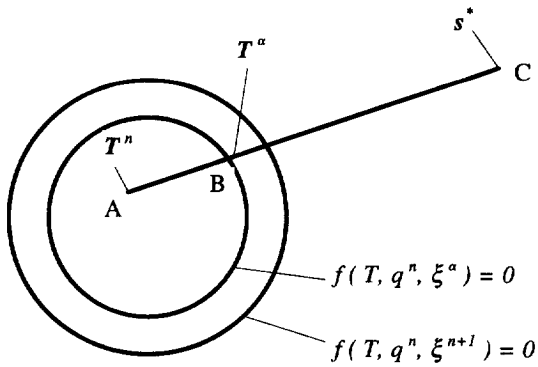

Fig. 5. On numerical integration of constitutive equations at elastoplastic deformation within a load increment.

points for stress calculation at the end of a load increment, Fig. 4(c). At first let us consider the case when the stress $\boldsymbol{T}^n$ lies within the yield surface, point A, Fig. 5. If the trial elastic deviatoric stress $\boldsymbol{s}^*$ lies outside the yield surface we get point $\subseteq$, Fig. 5. It means that during loading (the variables $\boldsymbol{F}$, $\boldsymbol{F}_t$, ξ are changing from values $\{\boldsymbol{F}^n, \boldsymbol{F}_t^n, \xi^n\}$ to $\{\boldsymbol{F}^{n+1}, \boldsymbol{F}_t^{n+1}, \xi^{n+1}\}$) a material point at first deforms elastically (line AB), then plastically (line BC). We assume that during load increment the variables $\boldsymbol{F}$, $\boldsymbol{F}_t$, ξ are changed proportionally to one scalar parameter κ, $0 \le \kappa \le 1$

$$\begin{aligned} \boldsymbol{F}^\kappa &= \boldsymbol{F}^n + \kappa(\boldsymbol{F}^{n+1} - \boldsymbol{F}^n), \\ \boldsymbol{F}_t^\kappa &= \boldsymbol{F}_t^n + \kappa(\boldsymbol{F}_t^{n+1} - \boldsymbol{F}_t^n), \\ \xi^\kappa &= \xi^n + \kappa(\xi^{n+1} - \xi^n). \end{aligned} \tag{62}$$

Then, the value $\kappa = \alpha$—corresponding to point B at the yield surface—can be computed by local iterations (like the consistency parameter λ in the radial return algorithm) from the following nonlinear algebraic equation

$$f(\boldsymbol{T}(\boldsymbol{F}^\alpha, \boldsymbol{F}_t^\alpha, \xi^\alpha), q^n, \xi^\alpha) = 0.$$

The stresses—corresponding to point B—are computed from the elastic law using known values of $\boldsymbol{F}^\alpha$, $\boldsymbol{F}_t^\alpha$, ξ^α. The remaining parts of the variables $\boldsymbol{F}$, $\boldsymbol{F}_t$, ξ are subdivided into m intervals according to the following formulas (so we have m intermediate points corresponding to plastic deformation process), Fig. 4(c),

$$\begin{aligned} \boldsymbol{F}^l &= \boldsymbol{F}^\alpha + \frac{l}{m}(\boldsymbol{F}^{n+1} - \boldsymbol{F}^\alpha), \\ \boldsymbol{F}_t^l &= \boldsymbol{F}_t^\alpha + \frac{l}{m}(\boldsymbol{F}_t^{n+1} - \boldsymbol{F}_t^\alpha), \\ \xi^l &= \xi^\alpha + \frac{l}{m}(\xi^{n+1} - \xi^\alpha), \\ l &= 1,2,\ldots,m. \end{aligned} \tag{63}$$

Then, we calculate subsequently $\{\boldsymbol{T}, q, \boldsymbol{F}_p\}^l$ in every intermediate point through the prescribed values of $\boldsymbol{F}^l$, $\boldsymbol{F}_t^l$, ξ^l according to the radial return algorithm up to the final values of $\{\boldsymbol{F}^{n+1}, \boldsymbol{F}_t^{n+1}, \xi^{n+1}\}$. Schematic subdivision of the deformation gradient, the transformation deformation gradient and the order parameter within a load increment is shown in Fig. 4(c). We can propose a simple formula for calculation of the number m

$$m = \frac{|\boldsymbol{s}^*| - \sqrt{\frac{2}{3}}\,\sigma_y(q^n, \xi^\alpha)}{\gamma_1 \sigma_y(q^n, \xi^\alpha)}$$

where $\boldsymbol{s}^*$ is the trial deviatoric stress for the final values of $\{\boldsymbol{F}\}^{n+1}$, ξ^{n+1}, $\{\boldsymbol{F}_t\}^{n+1}$; γ_1 is a small number which

can be found from the numerical experiment, for example $\gamma_1 = 0.1$. The cases when the stress T^n lies on the yield surface or the trial elastic deviatoric stress s^* lies within the yield surface are particular cases of such considered above.

REMARK 1. For the subdivision of the total and transformation deformation gradients into m parts we assume that $\boldsymbol{F}$ and $\boldsymbol{F}_t$ are proportionally changed with increasing the order parameter ξ during a load step, Eq. (63).

REMARK 2. The stresses computed in the intermediate points within a load step (points D_l, Fig. 4(c)) satisfy only constitutive equations but not the equilibrium equations. Only the stresses for the first and final points (corresponding to the beginning and the end of a load step, points A and C in Fig. 4(c)) fulfill the equilibrium equations, because we calculate residuals of the equilibrium equations and solve the global FE system of equations only for stresses at the end of a load step for point C, Fig. 4(c) (see below Section 3.2 and Box 3).

REMARK 3. The proposed numerical integration of the constitutive equations takes much less computer time than the solution of the global FE system of algebraic equations and does not increase essentially computing time. Such a modification can be used for any elastoplastic problem without PT as well.

3.2. General solution scheme and the consistent tangent moduli

The stresses $\boldsymbol{T}^{n+1}$ must satisfy the equilibrium equations which we enforce weakly using the principle of virtual work

$$\int_V \boldsymbol{T}^{n+1} : \left(\frac{\partial \boldsymbol{\eta}}{\partial \boldsymbol{r}}\right)_s \mathrm{d}V = \int_S \boldsymbol{t}^{n+1} \cdot \boldsymbol{\eta}\, \mathrm{d}S + \int_V \rho \boldsymbol{f}^{n+1} \cdot \boldsymbol{\eta}\, \mathrm{d}V, \tag{64}$$

where $\boldsymbol{t}^{n+1}$, $\boldsymbol{f}^{n+1}$ are the specified surface traction and body forces at time t_{n+1}; $\boldsymbol{\eta}$ are the virtual displacements; V, S are the volume and surface of a body in an actual configuration. As the stresses $\boldsymbol{T}^{n+1}$ can be expressed in terms of the deformation gradient $\boldsymbol{F}^{n+1}$ then solving Eq. (64) we can find $\boldsymbol{F}^{n+1}$ at time t_{n+1}. In order to use Newton–Raphson iterations for solving Eq. (64) (see Box 3 below) we need its linearized form. So, the rate form of the principle of virtual work (Eq. (64)) in actual configuration with the Cauchy stress tensor reads as follows (see Appendix)

$$\int_V \frac{\partial \boldsymbol{\eta}}{\partial \boldsymbol{r}} : \left(-\frac{\partial \boldsymbol{v}}{\partial \boldsymbol{r}} \cdot \boldsymbol{T}^{n+1} + \dot{\boldsymbol{T}}^{n+1} + \left(\boldsymbol{I} : \frac{\partial \boldsymbol{v}}{\partial \boldsymbol{r}}\right) \boldsymbol{T}^{n+1} \right) \mathrm{d}V = \int_S \boldsymbol{\eta} \cdot \left[\dot{\boldsymbol{t}} + \boldsymbol{t}^{n+1} \left(\boldsymbol{I} : \frac{\partial \boldsymbol{v}}{\partial \boldsymbol{r}} - \boldsymbol{N} \cdot \boldsymbol{d} \cdot \boldsymbol{N} \right) \right] \mathrm{d}S + \int_V \boldsymbol{\eta} \cdot \dot{\boldsymbol{f}} \rho\, \mathrm{d}V, \tag{65}$$

where $\boldsymbol{N}$ is the unit normal to the surface S. In order to use the left part of Eq. (65) for calculation of the tangent moduli we should express the rate of stresses $\boldsymbol{T}^{n+1}$ in terms of the velocity gradient $\partial \boldsymbol{v}/\partial \boldsymbol{r}$. Let us consider the derivation of such a formula which is consistent with the radial return algorithm for stress calculation with only one point integration within a load increment, Box 2. As $\boldsymbol{T}^{n+1}$ is a function of $\boldsymbol{\varepsilon}_e^*$ we can write

$$\dot{\boldsymbol{T}}^{n+1} = \frac{\partial \boldsymbol{T}^{n+1}}{\partial \boldsymbol{\varepsilon}_e^*} : \dot{\boldsymbol{\varepsilon}}_e^* = \frac{\partial \boldsymbol{T}^{n+1}}{\partial \boldsymbol{\varepsilon}_e^*} : \left(\frac{\partial \boldsymbol{\varepsilon}_e^*}{\partial \boldsymbol{F}} : \dot{\boldsymbol{F}} \right). \tag{66}$$

For isotropic elastoplastic materials with hardening the tensor $\partial \boldsymbol{T}^{n+1}/\partial \boldsymbol{\varepsilon}_e^*$ is the consistent tangent modulus for the case of small strains without PT [8,14] (because all the equations for their calculations are the same):

$$\boldsymbol{c}^{n+1} = \frac{\partial \boldsymbol{T}^{n+1}}{\partial \boldsymbol{\varepsilon}_e^*} = K(\xi^{n+1}) \boldsymbol{I} \otimes \boldsymbol{I} + 2G(\xi^{n+1}) \beta \left(\boldsymbol{II} - \frac{1}{3} \boldsymbol{I} \otimes \boldsymbol{I} \right) - 2G \bar{\gamma} \bar{\boldsymbol{n}} \otimes \bar{\boldsymbol{n}}, \tag{67}$$

where

$$\beta=\sqrt{\frac{2}{3}}\frac{\sigma_y(q^{n+1},\xi^{n+1})}{|\boldsymbol{s}^*|},\qquad \bar{\gamma}=\frac{1}{1+\dfrac{\dfrac{\partial\sigma_y(q^{n+1},\xi^{n+1})}{\partial q}}{3G(\xi^{n+1})}}-(1-\beta),\qquad \bar{\boldsymbol{n}}=\frac{\boldsymbol{s}^*}{|\boldsymbol{s}^*|} \tag{68}$$

and $\boldsymbol{II}$ is the fourth-order symmetric unit tensor with components $\frac{1}{2}(\delta_{ik}\ \delta_{jl}+\delta_{il}\delta_{jk})$. Dependence of elastic and plastic material parameters σ_y, G, K on the internal time ξ does not change the calculations because ξ is like loading parameter, and we prescribe it in advance at the beginning of every step, i.e. for every step we use the known values of K and G (which does not vary during a load step) and the known function $\sigma_y(q)$ at ξ^{n+1}.

To calculate $\dot{\varepsilon}_e^*$ in Eq. (66) we use some simplifications. Let us represent V_e^* as

$$V_e^*=\boldsymbol{I}+\tilde{\boldsymbol{\varepsilon}}_e^*. \tag{69}$$

Then expanding $\ln V_e^*$ in terms of $\tilde{\varepsilon}_e^*$ we get

$$\ln \boldsymbol{V}_e^*=\boldsymbol{\varepsilon}_e^*=\tilde{\boldsymbol{\varepsilon}}_e^*+\mathrm{O}(\tilde{\boldsymbol{\varepsilon}}_e^{*2}) \tag{70}$$

and we will neglect the term $\mathrm{O}(\tilde{\boldsymbol{\varepsilon}}_e^{*2})$ in the following equations. Differentiating the expression

$$\boldsymbol{F}_e^*\cdot(\boldsymbol{F}_e^*)^t=\boldsymbol{V}_e^*\cdot\boldsymbol{V}_e^*\approx\boldsymbol{I}+2\boldsymbol{\varepsilon}_e^* \tag{71}$$

with respect to time and taking into account

$$\dot{\boldsymbol{F}}_e^*=\dot{\boldsymbol{F}}\cdot\boldsymbol{F}_p^{-1}\cdot\boldsymbol{F}_t^{-1}=\dot{\boldsymbol{F}}\cdot\boldsymbol{F}^{-1}\cdot\boldsymbol{F}_e^*=\frac{\partial\boldsymbol{v}}{\partial\boldsymbol{r}}\cdot\boldsymbol{F}_e^* \tag{72}$$

we get

$$\dot{\boldsymbol{\varepsilon}}_e^*=\left(\frac{\partial\boldsymbol{v}}{\partial\boldsymbol{r}}\cdot\boldsymbol{V}_e^*\cdot\boldsymbol{V}_e^*\right)_s. \tag{73}$$

Then, the expression (66) takes the form

$$\dot{\boldsymbol{T}}^{n+1}=\boldsymbol{c}^{n+1}:\left(\frac{\partial\boldsymbol{v}}{\partial\boldsymbol{r}}\cdot\boldsymbol{V}_e^*\cdot\boldsymbol{V}_e^*\right)_s. \tag{74}$$

Now, we can represent the left part of Eq. (65) as follows:

$$\int_V\frac{\partial\boldsymbol{\eta}}{\partial\boldsymbol{r}}:\left(-\frac{\partial\boldsymbol{v}}{\partial\boldsymbol{r}}\cdot\boldsymbol{T}^{n+1}+\boldsymbol{c}^{n+1}:\left(\frac{\partial\boldsymbol{v}}{\partial\boldsymbol{r}}\cdot\boldsymbol{V}_e^*\cdot\boldsymbol{V}_e^*\right)_s+\left(\boldsymbol{I}:\frac{\partial\boldsymbol{v}}{\partial\boldsymbol{r}}\right)\boldsymbol{T}^{n+1}\right)\mathrm{d}V=\int_V\frac{\partial\boldsymbol{\eta}}{\partial\boldsymbol{r}}:\boldsymbol{k}^{n+1}:\frac{\partial\boldsymbol{v}}{\partial\boldsymbol{r}}\,\mathrm{d}V, \tag{75}$$

where $\boldsymbol{k}^{n+1}$ is the spatial consistent tangent determined by (75). The index form of $\boldsymbol{k}^{n+1}$ (in Cartesian coordinate system) reads as follows

$$k_{ijmn}^{n+1}=-T_{mj}\delta_{ni}+\frac{1}{2}c_{jiqp}^{n+1}(F_e^*)_{ml}(F_e^*)_{ql}\delta_{pn}+(F_e^*)_{ps}(F_e^*)_{ms}\delta_{qn})+T_{ij}\delta_{mn}. \tag{76}$$

The same terms on the right part of Eq. (65) is dependent on $\partial\boldsymbol{v}/\partial\boldsymbol{r}$. They are as follows

$$\int_S\boldsymbol{\eta}\cdot\boldsymbol{t}^{n+1}\left(\boldsymbol{I}:\frac{\partial\boldsymbol{v}}{\partial\boldsymbol{r}}-\boldsymbol{N}\cdot\boldsymbol{d}\cdot\boldsymbol{N}\right)\mathrm{d}S=\int_S\boldsymbol{\eta}\cdot\boldsymbol{k}_1^{n+1}:\frac{\partial\boldsymbol{v}}{\partial\boldsymbol{r}}\,\mathrm{d}S, \tag{77}$$

where $\boldsymbol{k}_1^{n+1}$ is determined by (77). The index form of $\boldsymbol{k}_1^{n+1}$ (in Cartesian coordinate system) is as follows

$$(k_1^{n+1})_{imn}=t_i(\delta_{mn}-N_nN_m). \tag{78}$$

Let us introduce index notations of tensors in the rectangular Cartesian coordinates system and the standard FE displacement approximations

$$\eta_i^h=\Psi_{i\beta}(x_m)\hat{\eta}_\beta,\qquad v_i^h=\Psi_{i\alpha}(x_m)\hat{v}_\alpha,\qquad \frac{\partial\eta_i^h}{\partial x_j}=\frac{\partial\Psi_{i\beta}}{\partial x_j}\hat{\eta}_\beta,\qquad \frac{\partial v_i^h}{\partial x_j}=\frac{\partial\Psi_{i\alpha}}{\partial x_j}\hat{v}_\alpha, \tag{79}$$

where $\Psi_{i\beta}(x_m)$ are the known interpolation functions, x_m are coordinates of a material point in the actual configuration, $\hat{\eta}_\beta$ and $\hat{v}_\alpha$ are the nodal values of components of the virtual displacement and velocity vectors; i, j, $m=1, 2, 3$; α, $\beta=1, 2,..., 3\times M$ (M is the number of nodes). Then, Eq. (64) can be rewritten as follows

$$\int_V [B]^t \{T\}^{n+1}\, dV - \{f\}^{n+1} = 0, \tag{80}$$

where

$$[B] = \frac{1}{2}\left(\frac{\partial \Psi_{i\beta}}{\partial x_j} + \frac{\partial \Psi_{j\beta}}{\partial x_i}\right)$$

is the standard finite element B-matrix for the current configuration (the same as for small strains),

$$(\{f\}^{n+1})_\beta = \int_S t_i^{n+1}\Psi_{i\beta}\, dS + \int_V \rho f_i^{n+1}\Psi_{i\beta}\, dV, \tag{81}$$

is the standard FE load vector. From expression

$$\int_V \frac{\partial \boldsymbol{\eta}}{\partial \boldsymbol{r}} : \boldsymbol{k}^{n+1} : \frac{\partial \boldsymbol{v}}{\partial \boldsymbol{r}}\, dV - \int_S \boldsymbol{\eta}\cdot \boldsymbol{k}_1^{n+1} : \frac{\partial \boldsymbol{v}}{\partial \boldsymbol{r}}\, dS, \tag{82}$$

which follows from Eqs. (65), (75) and (77), we get the consistent tangent stiffness matrix $[K]$

$$[K]_{\beta\alpha} = \int_V \frac{\partial \Psi_{i\beta}}{\partial x_j} k_{ijmn}^{n+1} \frac{\partial \Psi_{n\alpha}}{\partial x_m}\, dV - \int_S \Psi_{i\beta}\,(k_1^{n+1})_{imn} \frac{\partial \Psi_{n\alpha}}{\partial x_m}\, dS. \tag{83}$$

The global finite-element iteration procedure is briefly presented in Box 3.

REMARK 1. We can further modify Eq. (74) allowing for $\tilde{\boldsymbol{\varepsilon}}_e^* \ll \boldsymbol{I}$ at small increment of external load

$$\dot{\boldsymbol{T}}^{n+1} = \boldsymbol{c}^{n+1} : [(\boldsymbol{d}+\boldsymbol{W})\cdot(\boldsymbol{I}+2\tilde{\boldsymbol{\varepsilon}}_e^*)]_s \approx \boldsymbol{c}^{n+1} : (\boldsymbol{d}+\boldsymbol{W}\cdot 2\tilde{\boldsymbol{\varepsilon}}_e^*)_s, \tag{84}$$

where $\boldsymbol{W}=(\partial \boldsymbol{v}/\partial \boldsymbol{r})_a$ is the spin tensor. If the components of the tensor $\boldsymbol{d}$ have the same order or exceed the components of the tensor $\boldsymbol{W}$ then

$$\dot{\boldsymbol{T}}^{n+1} \approx \boldsymbol{c}^{n+1} : \boldsymbol{d}, \tag{85}$$

i.e. the structure of Eq. (85) is the same as for the case of small strains (but we consider large transformation—and plastic strains).

REMARK 2. It is necessary to note that approximate calculation of $\dot{\boldsymbol{\varepsilon}}_e^*$ (using Eqs. (70) and (71)) and hence $\boldsymbol{k}^{n+1}$ might affect the rate of convergence of the global iteration scheme but not the accuracy of the algorithm for stress calculation, Box 2.

The iteration procedure using the consistent tangents and the radial return algorithm with one integration point for stress calculations provides a fast decay of residual, but large load increments can violate the plastic flow rule (see Section 3.1 above). Therefore, to increase accuracy of the solution at large load increments and to preserve fast convergence, we propose the following modifications. The consistent tangents are always calculated with one integration point for the radial return algorithm. For stress calculations the radial return algorithm with one integration point can be used at initial iterations of the current load increment (2–4 iterations in order to obtain initial approximation of the solution). For subsequent iterations stresses should be computed with many integration point procedure described above (Section 3.1).

To determine the PT temperature we calculate the work integral Eq. $(24)_2$ in PT criterion (23). It can be done after solving the elastoplastic problem or during the solution process, i.e. the increment of the work integral for every loading step is calculated at the last iteration of every load step when the stress $\boldsymbol{T}$ in equilibrium is computed.

Box 3.
Finite element solution algorithm

1. Initialization at t_n. Data structure:
   Variables at quadrature points $\{q, F_p\}^n$
   Initial conditions for displacement vector at nodal points $\{u\}^{n+1}=0$
   Initial nodal coordinates $\{x\}^n$
   Current values of the order parameter ξ^{n+1}, the transformation deformation gradient $\{\boldsymbol{F}_t\}^{n+1}$ and boundary conditions

2. Let $\{u\}_k^{n+1}$ be solution at the k-iteration.
   2.1. Compute $\{F\}_k^{n+1}$ at quadrature points
   2.2. Compute $\{T, q, F_p\}_k^{n+1}$ at quadrature points according to the radial return algorithm and many integration point procedure
   2.3. Compute the consistent tangents at quadrature points.
   2.4. Compute residuals of the equilibrium equation $\{\Psi\}_k^{n+1}$ (see Eq. (64))

$$\{\Psi\}_k^{n+1}=\{f\}_k^{n+1}-\int_{V_k^{n+1}}([B]^t)_k^{n+1}\{T\}_k^{n+1}\,dV$$

   (for the current configuration and the Cauchy stress tensor the expression for $\{\Psi\}_k^{n+1}$ is the same as for small strains, $\{f\}_k^{n+1}$ is the standard FE load vector, $[B]_k^{n+1}$ is the standard B-matrix for finite elements with updated coordinates $\{x\}_k^{n+1}=\{x\}^n+\{u\}_k^{n+1}$)

   IF $\|\{\Psi\}_k^{n+1}\|<$ TOL GO TO 4 (TOL is a prescribed small number)

3. Solve system

$$[K]\{\Delta u\}_k^{n+1}=\gamma\{\Psi\}_k^{n+1},$$

   where $[K]$ is the consistent tangent stiffness matrix, γ is a parameter which is defined from numerical experiments, $\gamma\in[0,1]$. For the simplest case $\gamma=1$.
   Update $\{u\}_{k+1}^{n+1}=\{u\}_k^{n+1}+\{\Delta u\}_k^{n+1}$
   Set $k=k+1$ and GO TO 2

4. Update data structure
   $\{q, F_p\}^{n+1}=\{q, F_p\}_k^{n+1}$
   Update nodal coordinates $\{x\}^{n+1}=\{x\}_k^{n+1}$

REMARK 3. For increasing accuracy of stress–strain state calculation a mesh adaptivity can be used as it is done, for example, for elastoplastic problem at small strains in [24,25]. The development of such a procedure for finite elastoplastic strains with PT will be studied elsewhere.

REMARK 4. In the considered approach the PT region is assumed in advance and then the condition for PT in this region is determined, but in general case the PT region has to be computed. It can be done using extremum principle Eq. (25). For small strains the numerical procedure for determination of the progress of PT region due to changing external conditions (boundary conditions or (and) temperature) was proposed in [5]. It includes the determination of a sequence of small regions (each small region coincides with a finite element) where PT occurs, i.e. the whole PT region consists of all the small computed regions. The same procedure can be used as well for finite strains presented here. But a mathematical justification of this numerical scheme is open.

4. Numerical examples

To determine the conditions of martensitic PT and twinning in elastoplastic materials using PT criterion (23), we solve simple boundary–value problems. The following simplifying assumptions are presumed:

- elastic properties of matrix and nucleus are the same (for steel) : Young's modulus $E=2\cdot10^5$ MPa, Poisson ratio $\mu=0.3$.
- the case of plane strain state is considered;
- the inverse problem is solved, i.e. the position and size of the transforming region is specified a priori, and then the condition for PT is determined;
- the transformation deformation gradient in the transforming region (nucleus) increases homogeneously from the unit tensor to the final value according to Eq. (15);
- temperature is homogeneously distributed and does not change during PT, but it can change during elastoplastic deformations without PT.
- the critical driving force k_c is a constant or a function of temperature only.

Then, at given temperature, k_c and $\Delta\psi^\theta$ are known, hence the value of the work integral φ (due to PT condition (23)) gives full information for evaluating the possibility of PT.

For problems 4.1 and 4.2 the components of the transformation deformation gradient $\bar{\boldsymbol{F}}_t$ are prescribed in advance. For problem 4.3 we show the possibility of using the extremum principle Eq. $(25)_2$ to choose the favorable value of the transformation deformation gradient $\bar{\boldsymbol{F}}_t$. Quadratic triangles are used in calculations.

4.1. Appearance of a single martensitic plate in elastoplastic material

Here, we present an example of appearance of martensitic nucleus in elastoplastic material at finite strains. A similar problem for a representative volume of elastoplastic material was considered in a paper by Marketz and Fischer [4] for the case of small strains and another thermomechanical description of PT (using a simplified criterion for PT without taking into account the variation of stresses during PT). We also analyze and discuss a possible scenario of appearance of martensitic plate using the extremum principle for PT.

The cross section of a sample in plane strain state is given in Fig. 6. To evaluate the kind of martensitic plate formation (simultaneous appearance of a thin plate or appearance of a small nucleus and its subsequent growth) we carried out calculations for three cases of appearance of nucleus: (a) simultaneous PT in regions I–V (for the whole martensitic plate); (b) subsequent PT in regions I–V, i.e. first in region I, then in region II and so on; (c) appearance of one nucleus with different ratio of its width and length, i.e. PT occurs in region I, or simultaneously in regions I–II, or simultaneously in regions I–III and so on until simultaneous PT in regions I–V. The following plastic properties of steel are used in calculations [4]:

yield stress $\sigma_y^m=2.5\cdot10^2$ MPa for austenitic matrix and $\sigma_y^n=8\cdot10^2$ MPa for martensitic nucleus.

For simplicity we assume that yield stress in the nucleus changes instantaneously to the value of product phase after beginning of PT. The boundary of the sample is free from stresses which corresponds to experiments for temperature-induced PT. For our calculations the transformation deformation gradient $\bar{\boldsymbol{F}}_t$ and the order

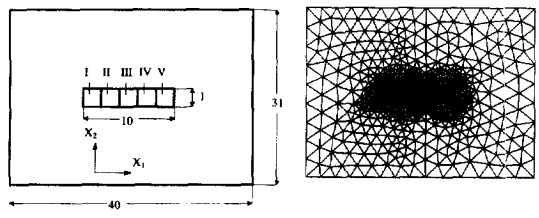

a b

Fig. 6. Cross-section (a) with stress-free boundary and FE mesh (b) of a sample with a nucleus (regions I–V).

parameter ξ are subdivided into 60 increments. $\bar{F}_t$ has the following components [4,17] in the Cartesian coordinate system with the normal n is directed along axes X_2, Fig. 6

$$(\bar{F}_t)_{11} = 1, \quad (\bar{F}_t)_{12} = 0.2, \quad (\bar{F}_t)_{21} = 0, \quad (\bar{F}_t)_{22} = 1.026, \quad (\bar{F}_t)_{33} = 1, \tag{86}$$

the other components are zero. Solving the elastoplastic problem with incrementally enlarged transformation deformation gradient we calculate stresses and the value of the work integral φ, and then from Eq. (23) one can find the PT temperature.

Results of calculations for simultaneous PT in regions I–V are presented in Fig. 7–10. The martensitic plate deforms practically elastically with the exception of small regions near short sides (Fig. 8(b)). In the parent phase the plastic strains are concentrated around the transformed plate (Fig. 8(a)). The shear stresses in the plate which make a main contribution to the work integral φ are distributed homogeneously in the central part and strongly inhomogeneously on periphery, Fig. 9. So, the analytical Eshelby solution for elastic materials at small strains which gives a homogeneous stress distribution within a plate deviates essentially from the real solution at finite elastoplastic strains (that was also indicated for the case of small elastoplastic strains in [4]). In Fig. 10 the variation of the work integral φ as a function of the order parameter ξ is shown, curve 1. We can use PT criterion (23) and the calculated value of the work integral $\varphi = -37$ MPa at $\xi = 1$ in order to determine the PT temperature, when the value of dissipative threshold k_c is known from experiment, or in order to determine k_c from the measurement of temperature for temperature-induced PT. If we use the data from Kaufman and Cohen [26] for steel Fe+30% Ni, then $\Delta\psi^{\theta}$ is -215.12 MPa at the martensite start temperature M_s, and according to Eq. (23) $k_c = 215.12 - 37 = 178.12$ MPa.

Now consider the second scenario of PT appearance when it occurs first in region I, then in region II and so on until the region V. The final value of the work integral, $\varphi \approx -71$ MPa at $\xi = 1$, is approximately the same for all five regions I–V (some of curves 2–6 coincide, Fig. 10); the value of the work integral $\varphi \approx -71$ MPa for PT in volume I is much smaller than $\varphi = -37$ MPa for the whole volume I–V (simultaneous appearance of the whole plate). According to extremum principle $(25)_2$ it means that simultaneous formation of thin martensitic plate is thermodynamically more favorable than appearance of a nucleus in a rectangular subdomain and its subsequent growth. The presence of stress concentrations (dislocations, grain boundaries) can, of course, change the scenario of nucleus appearance. In a simplified way we can simulate the presence of stress concentrators by a properly growing function $k_c(V_n)$ [2]. Then extremum principle (41) will result in appearance of a small nucleus.

The results for appearance of one nucleus with different ratio of its width and length are shown in Fig. 11 (case (c)). As we can see, the larger ratio $y = l/h$ (l and h are the length and width of a nucleus) is, the larger driving force for PT (the work integral φ, Fig. 11) is produced, but the dependence is nonlinear. A further reduction of the thickness of the transforming plate might be found by amendment of the physical model by a surface energy.

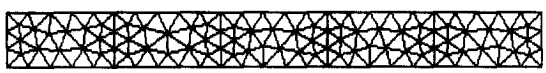

a

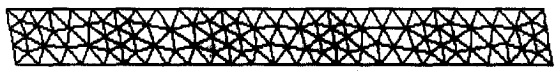

b

Fig. 7. FE meshes of regions I–V before (a) and after (b) PT at simultaneous PT in regions I–V.

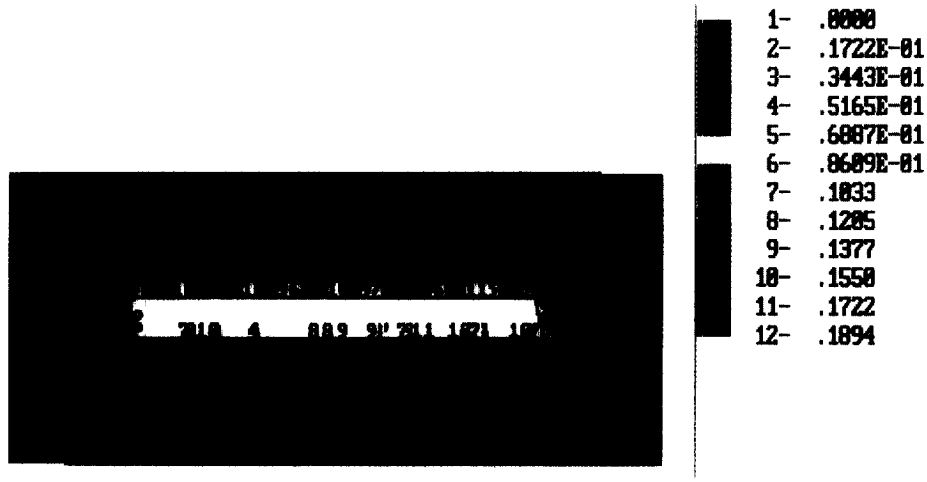

a

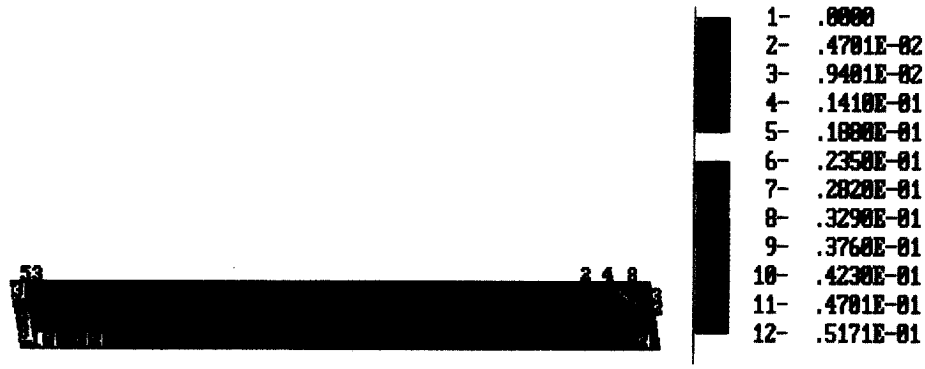

b

Fig. 8. Isobands of accumulated plastic strain q in a matrix near the martensitic plate (a) and in the martensitic plate (b) after PT.

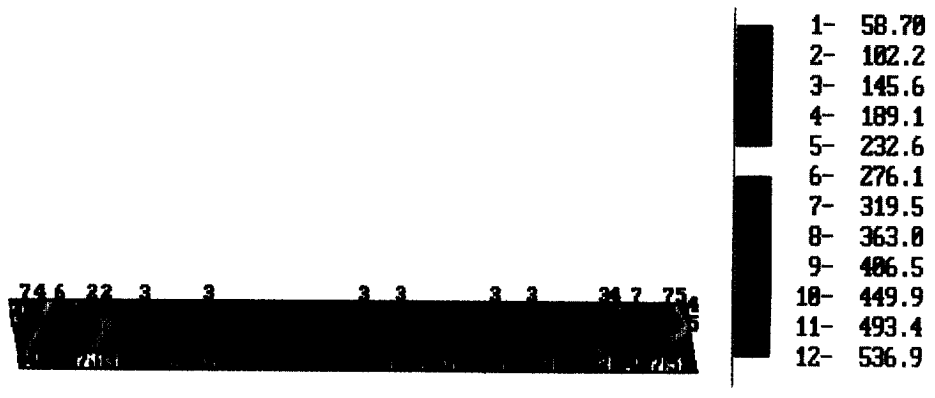

Fig. 9. Isobands of shear stress in the martensitic plate after PT.

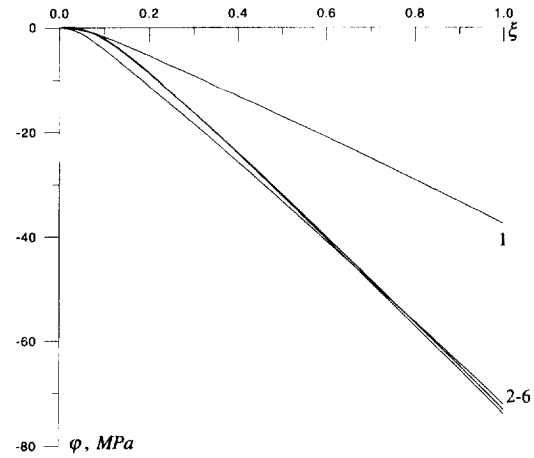

Fig. 10. Work integral as a function of ξ. Curve 1 corresponds to simultaneous PT in regions I–V, curves 2–6 correspond to subsequent PT in regions I–V.

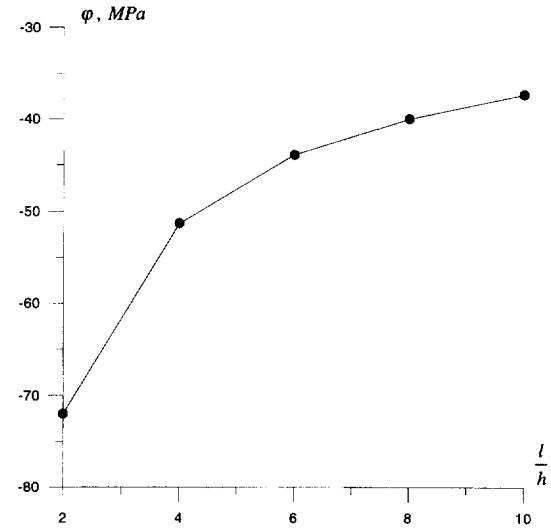

Fig. 11. Work integral as a function of a ratio l/h of the length l and width h of a nucleus.

4.2. Appearance of a single twin in elastoplastic material

As a model example, we consider appearance of a single twin caused by external stresses, Fig. 12. We take the same cross-section of a sample as for the previous problem, i.e. a twin forms a single plate in the parent phase. The differences from the previous problem are:

(a) the transformation deformation gradient has only a large shear component

$$(\bar{F}_t)_{11} = 1, \quad (\bar{F}_t)_{12} = 0.707, \quad (\bar{F}_t)_{21} = 0, \quad (\bar{F}_t)_{22} = 1, \quad (\bar{F}_t)_{33} = 1, \tag{87}$$

the other components are zero;

(b) the plastic properties of both phases are the same, and we analyze two cases with $\sigma_y = 4 \cdot 10^2$ MPa and $\sigma_y = 6 \cdot 10^2$ MPa;

(c) the thermal parts of the specific Helmholtz free energy for both phases are the same $\psi_1^\theta = \psi_2^\theta$;

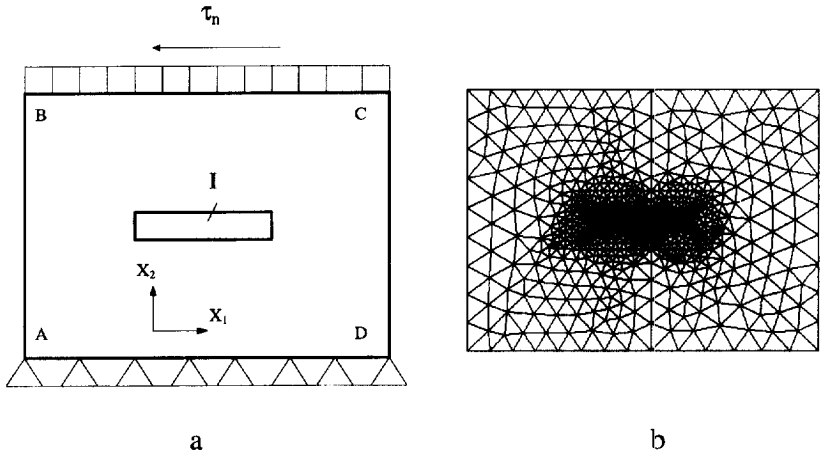

Fig. 12. Cross-section (a) and FE mesh (b) of a sample with a twin I.

We consider twin formation due to external shear stresses which are constant during the twinning. The following boundary conditions are applied:

- along BC boundary $u_n=0$, $\tau_n=180$ MPa;
- along AD boundary $u_n=u_\tau=0$;
- along AB and CD boundaries $\sigma_n=\tau_n=0$ (free surface),

where u_n and u_τ are the normal and tangential displacements, σ_n and τ_n are the normal and shear stresses.

The calculation of the work integral φ allows us to evaluate the possibility of twin formation, which yields—according to criterion (24)—that at $\varphi<k_c$ the appearance of a twin is impossible. The sequence of calculations is the same as for the problem with martensitic PT. For solving the elastoplastic problem the transformation deformation gradient $\boldsymbol{F}_t$ and the order parameter ξ are subdivided into 300 increments. Results of calculations are presented in Fig. 13–15. There we can see that the plastic strains are concentrated in the parent phase near the short sides of the transforming plate, Fig. 14. The shear stresses in the plate (Fig. 15) are homogeneously distributed in the central part and strongly inhomogeneously on periphery. In contrast to the previous problem 4.1, shear stresses (absolute values) in central part are smaller and they have the same sign as the external shear stresses. At the yield stress $\sigma_y=4\cdot10^2$ MPa the calculated value of the work integral φ is 30 MPa, Fig. 16, curve 1. If we know that a twin appears at applied shear stress $\tau_n=180$ MPa then we can evaluate the value of k_c, as according to criterion (24) $\varphi=k_c$ (k_c is a material parameter). Variation of the yield stress changes considerably the results. Such, solution of the same problem with another yield stress $\sigma_y=6\cdot10^2$ MPa yields $\varphi=-187$ MPa, Fig. 16, curve 2. It means that such a twin can not appear at $\tau_n=180$ MPa because the condition $\varphi=k\geq0$ is not met.

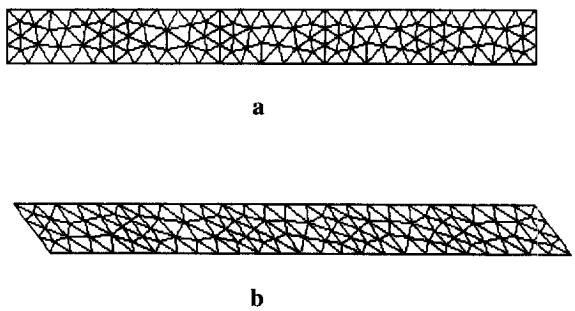

Fig. 13. FE mesh of the region I before (a) and after (b) twinning at $\sigma_y=400$ MPa.

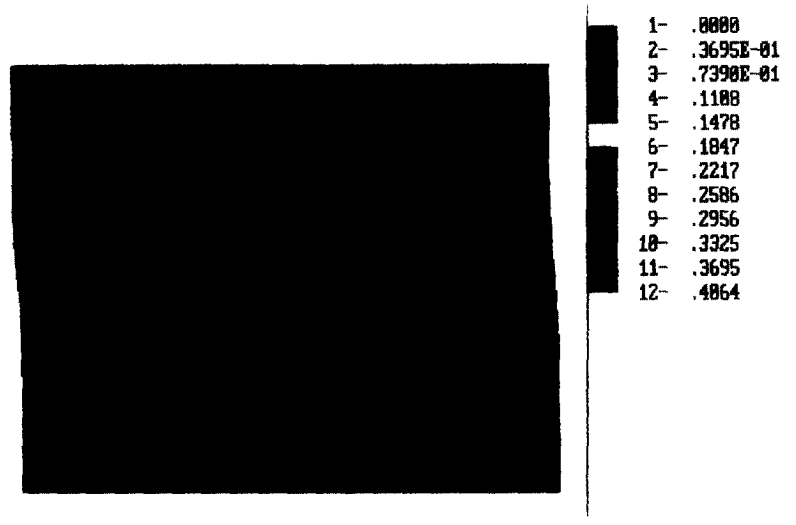

a

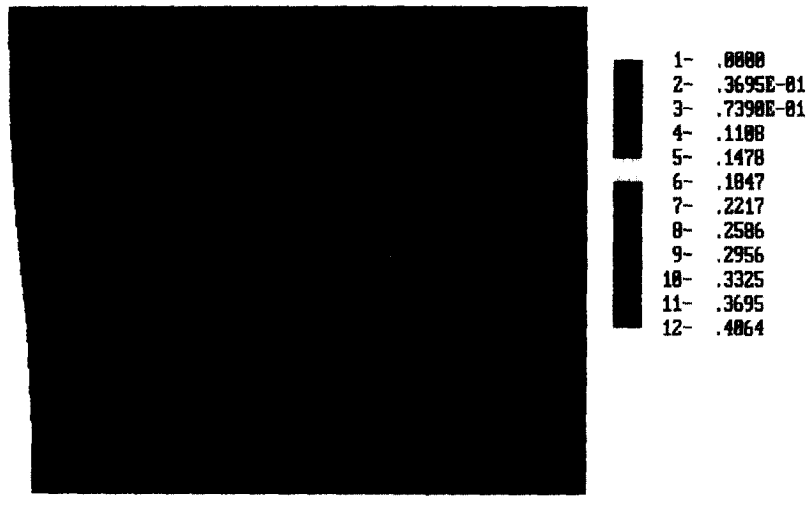

b

Fig. 14. Isobands of accumulated plastic strain q in a sample (a) and near a twin tip (b) at $\sigma_y = 400$ MPa.

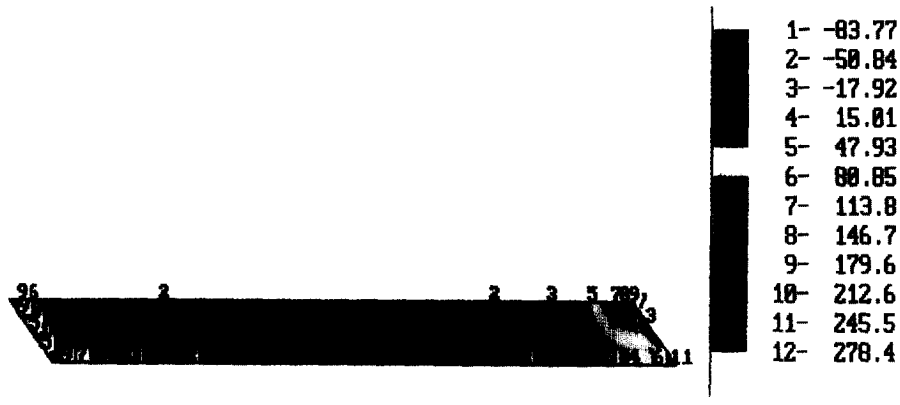

Fig. 15. Isobands of shear stress in a twin at $\sigma_y = 400$ MPa.

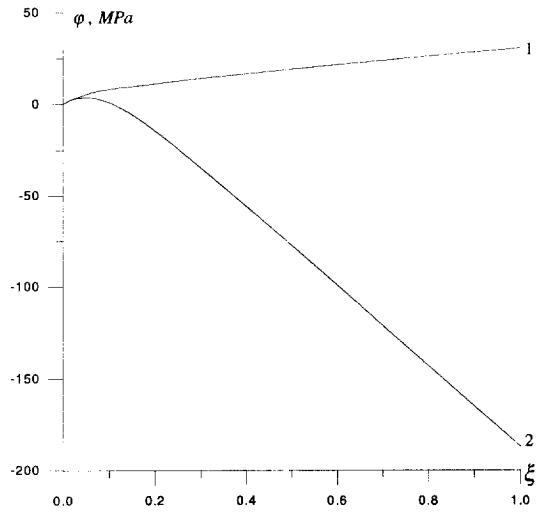

Fig. 16. Work integral φ as function of ξ during twinning (curve 1 at $\sigma_y = 400$ MPa, curve 2 at $\sigma_y = 600$ MPa).

4.3. Nucleation at shear–band intersection

It is known from experimental observations [27] that strain–induced PT occurs at shear band intersection. Let us consider the thermomechanical formulation of a model problem of nucleation at shear bands. Cross section of a sample is given in Fig. 17. The following presumptions hold: shear bands are introduced in advance; the material deforms elastoplastically within shear bands and elastically only outside shear bands. The plastic properties are the same as for the problem 4.1.

The following boundary conditions are applied:

- along AB boundary, $u_n = 0$, $\tau_n = 0$;
- along CD boundary, $u_n = u^*$, $\tau_n = 0$ (u^* is the prescribed normal displacement);
- along AC and BD, boundaries $\sigma_n = \tau_n = 0$ (free surface).

For calculations the transformation deformation gradient $\overline{\boldsymbol{F}}_t$ and the order parameter ξ are subdivided into 60 increments. In the local Cartesian coordinate system (one axis is directed along vector $\boldsymbol{n}$, another one is located in the plane of the vectors $\boldsymbol{n}$ and $\boldsymbol{k}$, i.e. in the plane of Fig. 17) the transformation deformation gradient $\overline{\boldsymbol{F}}_t$ has the following components

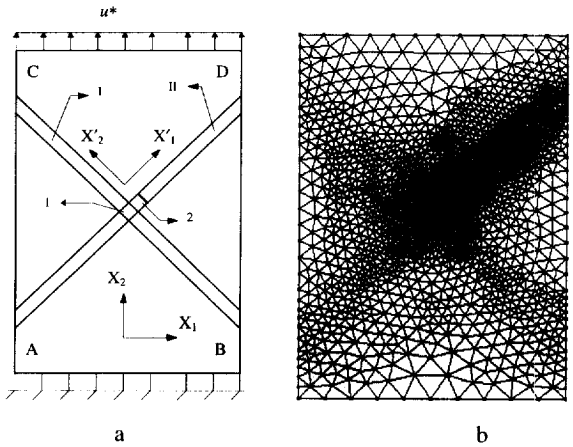

Fig. 17. Cross-section (a) and FE mesh (b) of a sample with a martensitic nucleus (1 or 2) at two shear-band (I and II) intersection.

$$(\bar{F}_t)_{11} = 1, \quad (\bar{F}_t)_{12} = 0.2, \quad (\bar{F}_t)_{21} = 0, \quad (\bar{F}_t)_{22} = 1.026, \quad (\bar{F}_t)_{33} = 1, \tag{88}$$

the other components are zero.

Four different values of maximal prescribed displacement u^*_{max} are considered, namely

$$u^*_{max} = 0.14; \quad 0.19; \quad 0.24; \quad 0.34, \tag{89}$$

which correspond to the following macroscopic tensile strain

$$\varepsilon = u^*_{max}/h = 0.0047; \quad 0.0063; \quad 0.0080; \quad 0.0113, \tag{90}$$

where $h=30$ is the initial height of the sample. During PT the transformation deformation gradient and prescribed displacements grow proportionally to the order parameter ξ,

$$u^*(\xi) = u^*_1 + (u^*_{max} - u^*_1)\xi, \tag{91}$$

i.e. it means that the transformation deformation gradient grows proportionally to the prescribed displacement. For all cases we start PT at $\varepsilon = u^*_1/h = 0.14\%$ when plastic strains appear in shear–band regions. This corresponds to the situation where transformation occurs during the shear–band intersection event. The beginning of PT can be enforced by variation of temperature.

For this problem we assume that the transformation gradient $\bar{F}_t$ is determined up to arbitrary rotation (see Remark 3, Section 2.1). For the considered plane case it means that the direction of the normal n with respect to the global coordinate system is unknown. We find the most favorable one using the extremum principle $(25)_2$. Four different angles were prescribed $\alpha = 0$; 45°; 50°; 90° between n and axis X_2, Fig. 17. Solving four boundary–value problems for the $u^*_{max} = 0.24$ and appearance of martensite at the shear–band intersection we have found that the corresponding values of the work integral φ are $\varphi = -36.86$; 22.59; 21.86; -37.06 MPa, respectively. According to the extremum principle (25), the most favorable direction for the vector $\boldsymbol{n}$ is along one of the shear bands (along the axis X'_2, Fig. 17), since for this direction the work integral $\varphi = 22.59$ has a maximum value. In the following calculation we use this direction for prescribing the transformation deformation gradient $\bar{F}_t$. Then, the transformation deformation gradient $\bar{F}_t$ has the components Eq. (88) in the local coordinate system in which axes are directed along shear bands.

REMARK. For an infinite number of variants for the angle between $\boldsymbol{n}$ and axis X_2 the check of a discrete number of possible values gives an approximate solution. If we use in three-dimensional case the model with a finite number of variants for $\bar{F}_t$, then such a check allows to find the true variant.

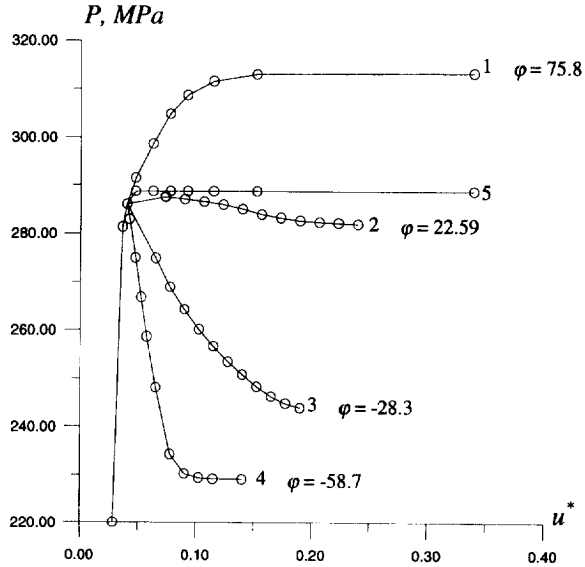

Fig. 18. Relationships between external averaged axial stress P and vertical displacement u^* (at different values u^* after finishing PT). (1) work integral $\varphi = 75.8$ MPa, (2) $\varphi = 22.59$ MPa, (3) $\varphi = -28.3$ MPa, (4) $\varphi = -58.7$ MPa, (5) without PT.

In Fig. 18 the relationship between external averaged axial stress (obtained from the problem solution and averaged over boundary CD) and vertical displacement at boundary CD is shown and computed values of the work integral φ are indicated. Curves 1–4 correspond to appearance of nucleus at shear band intersection, curve 5 describes deformation without PT. The growth of axial stress for curve 1 is explained by the fact that yield stress for nucleus is higher than for matrix.

Using PT criterion (23) and the value of the work integral φ (for curve 2–4) we can calculate the PT temperature. If the temperature is given then using the value of the work integral φ we can predict whether PT occurs. For normal displacement $u^*_{\max}=0.19$ at boundary CD we have solved also the problem with appearance of nucleus in volume 2, Fig. 17 (volumes 1 and 2 are equal). The work integral is $\varphi=-42.2$ MPa for this case, i.e. the PT driving force $\bar{X}$ for nucleus at shear band intersection (volume 1, $\varphi=-28.3$ MPa) is higher than for nucleus in volume 2, and—due to extremum principle $(25)_2$—PT will occur at the same external conditions in volume 1 at shear band intersection. We also have solved the problem when after nucleation in volume 1, PT occurs in volume 2 (i.e. the growth of nucleus 1 is modelled). But the value of the work integral φ for volume 2 was much smaller than φ for volume 1 of initial nucleus. This means impossibility of growth of nucleus 1 because the appearance of nucleus at intersection of other shear bands is more favorable. This corresponds to the known experimental observations [27].

5. Concluding remarks

The description of martensitic PT in elastoplastic materials is mathematically much more complicated than in elastic materials without dissipation due to dependence of PT conditions on the history of stress–strain changes in nucleus during PT. Three model problems were solved by introducing some simplifying reasonable assumptions. Numerical algorithm and solution are given, determining the appearance of a nucleus in some model problems. Due to the formulation of 'inverse' problem—when the PT region is prescribed in advance—the main computational difficulty lies in calculation of stress changes in the prescribed transforming region in course of PT at finite plastic and transformation strains. The usage of the current configuration and the true Cauchy stresses together with the assumptions of small elastic strains and zero plastic spin allow us to use—with small modifications—the radial return algorithm and the consistent elastoplastic moduli for the case of small strains. Numerical algorithm developed for PT also can be used for thermoelastoplasticy at finite strains due to the similarity of formulations.

Acknowledgement

We gratefully acknowledge the support of the VOLKSWAGEN FOUNDATION, grant I/70283.

Appendix A. Derivation of the rate form of the principle of virtual work

The principle of virtual work in a deformed configuration at an arbitrary time t is given in the form

$$\int_V \boldsymbol{T}:\left(\frac{\partial \boldsymbol{\eta}}{\partial \boldsymbol{r}}\right)_s \mathrm{d}V=\int_S \boldsymbol{t}\cdot\boldsymbol{\eta}\,\mathrm{d}S+\int_V \rho\boldsymbol{f}\cdot\boldsymbol{\eta}\,\mathrm{d}V, \tag{A.1}$$

where $\boldsymbol{T}$ is the Cauchy stress tensor; $\boldsymbol{t}$, $\boldsymbol{f}$ are the specified surface traction and body forces; $\boldsymbol{\eta}$ are the virtual displacements, ρ is the density; V, S are the volume and surface of a body in a deformed configuration; $\boldsymbol{r}$ is the position vector of a point at time t. With respect to an arbitrary initial configuration at time t_o Eq. (A.1) takes the form

$$\int_{V_o} \boldsymbol{T}:\frac{\partial \boldsymbol{\eta}}{\partial \boldsymbol{r}_o}\cdot\frac{\partial \boldsymbol{r}_o}{\partial \boldsymbol{r}}\frac{\mathrm{d}V}{\mathrm{d}V_o}\,\mathrm{d}V_o=\int_{S_o} \boldsymbol{t}\cdot\boldsymbol{\eta}\frac{\mathrm{d}S}{\mathrm{d}S_o}\,\mathrm{d}S_o+\int_{V_o} \boldsymbol{f}\cdot\boldsymbol{\eta}\rho_o\,\mathrm{d}V_o, \tag{A.2}$$

where $\boldsymbol{r}_o$ is the position vector of a point at time t_o, index 'o' designates the initial configuration at time t_o. To

express principle (A.1) in rate form for a deformed configuration we differentiate Eq. (A.2) in the time-independent initial configuration at time t_o, and then we again pass to a deformed configuration at time t. First, we differentiate Eq. (A.2)

$$\int_{V_o} \frac{\partial \dot{\boldsymbol{\eta}}}{\partial \boldsymbol{r}_o} : \left(\frac{\partial \boldsymbol{r}_o}{\partial \boldsymbol{r}} \cdot \boldsymbol{T} \frac{\mathrm{d}V}{\mathrm{d}V_o}\right) \mathrm{d}V_o + \int_{V_o} \frac{\partial \boldsymbol{\eta}}{\partial \boldsymbol{r}_o} : \overline{\left(\frac{\partial \boldsymbol{r}_o}{\partial \boldsymbol{r}} \cdot \boldsymbol{T} \frac{\mathrm{d}V}{\mathrm{d}V_o}\right)}\, \mathrm{d}V_o$$

$$= \int_{S_o} \dot{\boldsymbol{\eta}} \cdot \left(t \frac{\mathrm{d}S}{\mathrm{d}S_o}\right) \mathrm{d}S_o + \int_{S_o} \boldsymbol{\eta} \cdot \overline{\left(t \frac{\mathrm{d}S}{\mathrm{d}S_o}\right)}\, \mathrm{d}S_o + \int_{V_o} \dot{\boldsymbol{\eta}} \cdot \boldsymbol{f} \rho_o \, \mathrm{d}V_o + \int_{V_o} \boldsymbol{\eta} \cdot \dot{\boldsymbol{f}} \rho_o \, \mathrm{d}V_o. \tag{A.3}$$

As $\dot{\boldsymbol{\eta}}$ is arbitrary and taking into account Eq. (A.2), it follows that the first, the third and the fifth terms in Eq. (A.3) cancel out. Then

$$\int_{V_o} \frac{\partial \boldsymbol{\eta}}{\partial \boldsymbol{r}_o} : \overline{\left(\frac{\partial \boldsymbol{r}_o}{\partial \boldsymbol{r}} \cdot \boldsymbol{T} \frac{\mathrm{d}V}{\mathrm{d}V_o}\right)}\, \mathrm{d}V_o = \int_{S_o} \boldsymbol{\eta} \cdot \overline{\left(t \frac{\mathrm{d}S}{\mathrm{d}S_o}\right)}\, \mathrm{d}S_o + \int_{V_o} \boldsymbol{\eta} \cdot \dot{\boldsymbol{f}} \rho_o \, \mathrm{d}V_o. \tag{A.4}$$

Rewriting Eq. (A.4) for a deformed configuration at time t we get

$$\int_{V} \frac{\partial \boldsymbol{\eta}}{\partial \boldsymbol{r}} \cdot \frac{\partial \boldsymbol{r}}{\partial \boldsymbol{r}_o} : \overline{\left(\frac{\partial \boldsymbol{r}_o}{\partial \boldsymbol{r}} \cdot \boldsymbol{T} \frac{\mathrm{d}V}{\mathrm{d}V_o}\right)}\, \frac{\mathrm{d}V_o}{\mathrm{d}V} \mathrm{d}V = \int_{S} \boldsymbol{\eta} \cdot \overline{\left(t \frac{\mathrm{d}S}{\mathrm{d}S_o}\right)}\, \frac{\mathrm{d}S_o}{\mathrm{d}S} \mathrm{d}S + \int_{V} \boldsymbol{\eta} \cdot \dot{\boldsymbol{f}} \rho \, \mathrm{d}V. \tag{A.5}$$

Let $\boldsymbol{F} = \partial \boldsymbol{r} / \partial \boldsymbol{r}_o$ be the deformation gradient and $\boldsymbol{G} = \boldsymbol{F}^{\mathrm{t}} \cdot \boldsymbol{F}$ (right Cauchy–Green tensor). Then $\mathrm{d}V/\mathrm{d}V_o = \sqrt{I_3(\boldsymbol{G})}$, where $I_3(\boldsymbol{G})$ is the third invariant of the tensor $\boldsymbol{G}$ [28].

Let us consider the subintegral expression in the left hand part of Eq. (A.5).

$$\frac{\partial \boldsymbol{\eta}}{\partial \boldsymbol{r}} \cdot \frac{\partial \boldsymbol{r}}{\partial \boldsymbol{r}_o} : \overline{\left(\frac{\partial \boldsymbol{r}_o}{\partial \boldsymbol{r}} \cdot \boldsymbol{T} \frac{\mathrm{d}V}{\mathrm{d}V_o}\right)}\, \frac{\mathrm{d}V_o}{\mathrm{d}V} \mathrm{d}V = \frac{\partial \boldsymbol{\eta}}{\partial \boldsymbol{r}} : \boldsymbol{F} \cdot \Big(\dot{\boldsymbol{F}}^{-1} \cdot \boldsymbol{T} \sqrt{I_3(\boldsymbol{G})} + \boldsymbol{F}^{-1} \cdot \dot{\boldsymbol{T}} \sqrt{I_3(\boldsymbol{G})} + \boldsymbol{F}^{-1}$$

$$\cdot \boldsymbol{T} \overline{\sqrt{I_3(\boldsymbol{G})}}\Big) \frac{1}{\sqrt{I_3(\boldsymbol{G})}} = \frac{\partial \boldsymbol{\eta}}{\partial \boldsymbol{r}} : \left(\boldsymbol{F} \cdot \dot{\boldsymbol{F}}^{-1} \cdot \boldsymbol{T} + \dot{\boldsymbol{T}} + \boldsymbol{T} \frac{\overline{\sqrt{I_3(\boldsymbol{G})}}}{\sqrt{I_3(\boldsymbol{G})}}\right)$$

$$= \frac{\partial \boldsymbol{\eta}}{\partial \boldsymbol{r}} : \Big(- \frac{\partial \boldsymbol{v}}{\partial \boldsymbol{r}} \cdot \boldsymbol{T} + \dot{\boldsymbol{T}} + \Big(\boldsymbol{I} : \frac{\partial \boldsymbol{v}}{\partial \boldsymbol{r}}\Big) \boldsymbol{T}\Big). \tag{A.6}$$

Here we have used that $\dot{\boldsymbol{F}}^{-1} = -\boldsymbol{F}^{-1} \cdot \dot{\boldsymbol{F}} \cdot \boldsymbol{F}^{-1}$ (which follows from the differentiation of the relation $\boldsymbol{F} \cdot \boldsymbol{F}^{-1} = \boldsymbol{I}$, where $\boldsymbol{I}$ is the unit tensor), and that $\dot{\boldsymbol{F}} \cdot \boldsymbol{F}^{-1} = \partial \boldsymbol{v} / \partial \boldsymbol{r}$, $\overline{\sqrt{I_3(\boldsymbol{G})}} / \sqrt{I_3(\boldsymbol{G})} = \boldsymbol{I} : \frac{\partial \boldsymbol{v}}{\partial \boldsymbol{r}}$, where $\boldsymbol{v} = \dot{\boldsymbol{r}}$ is the velocity [28].

Now we consider the first expression in the right-hand part of Eq. (A.5). Taking into account that

$$\overline{\left(\frac{\mathrm{d}S}{\mathrm{d}S_o}\right)} = \frac{\mathrm{d}S}{\mathrm{d}S_o} \Big(\boldsymbol{I} : \frac{\partial \boldsymbol{v}}{\partial \boldsymbol{r}} - \boldsymbol{N} \cdot \boldsymbol{d} \cdot \boldsymbol{N}\Big), \tag{A.7}$$

where $\boldsymbol{d} = (\partial \boldsymbol{v} / \partial \boldsymbol{r})_s$, $\boldsymbol{N}$ is the unit normal to the surface $\mathrm{d}S$ [28], one obtains

$$\int_{S} \boldsymbol{\eta} \cdot \overline{\left(t \frac{\mathrm{d}S}{\mathrm{d}S_o}\right)}\, \frac{\mathrm{d}S_o}{\mathrm{d}S} \mathrm{d}S = \int_{S} \boldsymbol{\eta} \cdot \left[\dot{t} \frac{\mathrm{d}S}{\mathrm{d}S_o} + t \overline{\frac{\mathrm{d}S}{\mathrm{d}S_o}}\right] \frac{\mathrm{d}S_o}{\mathrm{d}S} \mathrm{d}S = \int_{S} \boldsymbol{\eta} \cdot \left[\dot{t} + t \Big(\boldsymbol{I} : \frac{\partial \boldsymbol{v}}{\partial \boldsymbol{r}} - \boldsymbol{N} \cdot \boldsymbol{d} \cdot \boldsymbol{N}\Big)\right] \mathrm{d}S. \tag{A.8}$$

Thus, the final rate form of the principle of virtual work is as follows

$$\int_{V} \frac{\partial \boldsymbol{\eta}}{\partial \boldsymbol{r}} : \Big(- \frac{\partial \boldsymbol{v}}{\partial \boldsymbol{r}} \cdot \boldsymbol{T} + \dot{\boldsymbol{T}} + \Big(\boldsymbol{I} : \frac{\partial \boldsymbol{v}}{\partial \boldsymbol{r}}\Big) \boldsymbol{T}\Big) \mathrm{d}V = \int_{S} \boldsymbol{\eta} \cdot \left[\dot{t} + t \Big(\boldsymbol{I} : \frac{\partial \boldsymbol{v}}{\partial \boldsymbol{r}} - \boldsymbol{N} \cdot \boldsymbol{d} \cdot \boldsymbol{N}\Big)\right] \mathrm{d}S + \int_{V} \boldsymbol{\eta} \cdot \dot{\boldsymbol{f}} \rho \, \mathrm{d}V. \tag{A.9}$$

As $\boldsymbol{T}$ and $\dot{\boldsymbol{T}}$ are symmetrical tensors we can use simplification

$$\frac{\partial \boldsymbol{\eta}}{\partial \boldsymbol{r}} : \Big(\dot{\boldsymbol{T}} + \Big(\boldsymbol{I} : \frac{\partial \boldsymbol{v}}{\partial \boldsymbol{r}}\Big)\boldsymbol{T}\Big) = \Big(\frac{\partial \boldsymbol{\eta}}{\partial \boldsymbol{r}}\Big)_s : \Big(\dot{\boldsymbol{T}} + \Big(\boldsymbol{I} : \frac{\partial \boldsymbol{v}}{\partial \boldsymbol{r}}\Big)\boldsymbol{T}\Big).$$

In order to use Eq. (A.9) for derivation of the tangent stiffness matrix we express the rate of stresses $\dot{\boldsymbol{T}}$ in terms of the velocity gradient $\partial \boldsymbol{v}/\partial \boldsymbol{r}$, see Section 3.2.

References

[1] V.I. Levitas, Phase transitions in inelastic materials at finite strains: a local description, Journal de Physique IV, Colloque C1, supplement au J. de Physique III 6 (1996) 55–64.

[2] V.I. Levitas, Thermomechanical theory of martensitic phase transformations in inelastic materials, Int. J. Solid Struct. 35(9–10) (1998) 889–940.

[3] J.F. Ganghoffer, S. Denis, E. Gautier, A. Simon, K. Simonsson and S. Sjöström, Micromechanical simulation of a martensitic transformation by finite element, Journal de Physique IV, Colloque C4 1 (1991) 83–88.

[4] F. Marketz and F. D. Fischer, Micromechanical modelling of stress-assisted martensitic transformation, Modelling Simul. Mater. Sci. Engrg. 2 (1994) 1017.

[5] V.I. Levitas, A.V. Idesman and E. Stein, Finite element simulation of martensitic phase transitions in elastoplastic materials, Int. J. Solid Struct. 35 (9–10) (1998) 855–887.

[6] G. Reisner, Micromechanical modelling of strain induced martensitic transformation in Cu-Fe alloys and in low alloyed TRIP-steels. Fortshr.-Ber. VDI Reihe 18 Nr. 214. Düsseldorf: VDI Verlag (1997).

[7] A.V. Idesman, V.I. Levitas and E. Stein, Simulation of martensitic phase transition progress with continuous and discontinuous displacements at the interface, Comput. Mat. Sci. 9 (1997) 64–75.

[8] J.C. Simo and T.J.R. Hughes, Elastoplasticity and Viscoplasticity—Computational Aspects, Springer Ser. Appl. Math. (Springer, Berlin, 1989).

[9] J.C. Simo and C. Miehe, Associative coupled thermoplasticity at finite strains: Formulation, numerical analysis and implementation, Comput. Methods Appl. Mech. Engrg. 98 (1992) 41–104.

[10] G. Weber, L. Anand, Finite deformation constitutive equations and a time integration procedure for isotropic hyperelastic-viscoplastic solids, Comput. Methods Appl. Mech. Engrg. 79 (1990) 173–202

[11] A. Cuitino and M. Ortiz, A material-independent method for extending stress update algorithms from small-strain plasticity to finite with multiplicative kinematics, Engrg. Comput. 9 (1992) 437–451.

[12] A.V. Idesman, V.I. Levitas and E. Stein, Finite element simulation of martensitic phase transition in elastoplastic material at finite strains, in: D.R.J. Owen, E. Oñate, E. Hilton, eds., Computational Plasticity. Fundamentals and Applications. Part 2. Proc. Fifth Int. Conf. on Computational Plasticity. Barcelona, Spain (1997) 1323–1328.

[13] A.V. Idesman, V.I. Levitas and E. Stein, Elastoplastic materials with martensitic phase transition at finite strains: numerical simulation, in: O.T. Bruhns, E. Stein, eds., Proc. IUTAM Symposium on Micro- and Macrostructural Aspects of Thermoplasticity, Bochum, Germany, 1997 (Kluwer, Dordrecht, 1999 (373–382).

[14] J.C. Simo and R.T. Taylor, Consistent tangent operators for rate-independent elastoplasticity, Comput. Methods Appl. Mech. Engrg. 48 (1985) 101–118.

[15] E.M. Morozov and G.P. Nikishkov, FEM in Fracture Mechanics (Nauka, Moscow, 1980) [in Russian].

[16] J.W. Christian, The Theory of Transformation in Metals and Alloys (Pergamon Press, Oxford, 1965).

[17] Z. Nishiyama, Martensitic Transformation (Academic Press, New York, 1978).

[18] J.M. Ball and R.D. James, Proposed experimental tests of a theory of fine microstructure and the two–well problem, Phil. Trans. Roy. Soc. Lond. A. 338A (1992) 389–450.

[19] K. Bhattacharya and R.V. Kohn, Recoverable strains in shape–memory polycrystals. Journal de Physique IV, Colloque C8, supplément au J. de Physique III 5 (1995) 261–266.

[20] V.I. Levitas, Large deformation of materials with complex rheological properties at normal and high pressure (Nova Science Publishers, New York, 1996).

[21] Y. Huo and I. Müller, Thermodynamics of pseudoelasticity—a graphical approach, Continuum Mech. Thermodyn. 5 (1993) 163–204.

[22] V.I. Levitas, The postulate of realizability: formulation and applications to post–bifurcation behavior and phase transitions in elastoplastic materials, Parts I and II, Int. J. Engrg. Sci. 33 (1995) 921–971.

[23] A.V. Idesman and V.I. Levitas, Finite element procedure for solving contact thermoplastic problems at large strain, normal and high pressures, Comput. Methods. Appl. Mech. Engrg. 126 (1995) 39–66.

[24] F.–J. Barthold, M. Schmidt and E. Stein, Error indicators and mesh refinements for finite-element-computations of elastoplastic deformations, in: D.R.J. Owen, E. Oñate, E. Hilton, eds., Computational Plasticity. Fundamentals and Applications. Part I, Proc. Fifth Int. Conf. on Computational Plasticity. Barcelona, Spain (1997) 597–602.

[25] F.-J. Barthold, M. Schmidt and E. Stein, Error indicators and mesh refinements for finite-element-computations of elastoplastic deformations, Comput. Mech. 22 (1998) 225–238.

[26] L. Kaufman and M. Cohen, Thermodynamics and kinetics of martensitic transformations, in: B. Chalmers and R. King, eds., Progress in Metal Physics (Pergamon Press, London et al., 1958) 165–246.

[27] R.G. Stringfellow, D.M. Parks and G.B. Olson, A constitutive model for transformation plasticity accompanying strain–induced martensitic transformations in metastable austenitic steels, Acta Metall. Mater. 40 (1992) 1703–1716.

[28] A.I. Lurie, Nonlinear Theory of Elasticity (North-Holland, Amsterdam, 1990).